NASA
Technical
Paper
2700

May 1987

Wind-Tunnel Free-Flight Investigation of a 0.15-Scale Model of the F-106B Airplane With Vortex Flaps

Long P. Yip

NASA

NASA Technical Paper 2700

1987

Wind-Tunnel Free-Flight Investigation of a 0.15-Scale Model of the F-106B Airplane With Vortex Flaps

Long P. Yip

Langley Research Center
Hampton, Virginia

National Aeronautics and Space Administration

Scientific and Technical Information Office

Introduction

Vortex flaps have been studied in many theoretical and experimental research investigations (for example, refs. 1 to 7) as a means of controlling the formation of vortical flow along the leading edges of highly swept wing surfaces. Much of the research on vortex flap aerodynamics was highlighted in a recent conference held at the Langley Research Center (ref. 8). Research has shown vortex flaps to be a very promising concept for achieving improved subsonic and transonic maneuver performance of highly swept wing configurations. The vortex flap concept would be particularly applicable to advanced fighters that need a combination of good supersonic cruise capability and high subsonic and transonic maneuver capability.

As part of the vortex flap validation effort, a flight test is planned on the F-106B airplane to document the aerodynamics of vortex flap design (fig. 1). In anticipation of the flight validation program, a series of wind-tunnel tests (see fig. 2) have been conducted to assess the impact of vortex flaps on the aerodynamic characteristics of the F-106B airplane configuration (refs. 9 and 10). The overall objectives of these investigations were to develop a data base for the design and analysis of vortex flaps and to provide airplane aerodynamic data for use in the analysis of the flight test validation of the F-106B vortex flap configuration.

In the area of low-speed, high-angle-of-attack flight research, the approach used to obtain these objectives is illustrated in figure 3. Static force tests and dynamic forced-oscillation tests are conducted with supporting flow visualization studies to determine the aerodynamic impact of vortex flaps on the F-106B configuration. Free-flight testing is used in addition to provide flight characteristics and to identify any potential problem areas not identified by the static or dynamic data for $1g$ flight on a dynamically scaled model up to the stall angle of attack. Flight characteristics and handling qualities are further investigated through the use of piloted-simulation studies. A complete aerodynamic data set, including low-speed and high-speed aerodynamic characteristics, is incorporated in piloted-simulation studies to assess the impact of vortex flaps on the handling qualities throughout the planned flight envelope from takeoff to maneuvering flight and back to landing approach.

The purpose of this investigation is to provide information on the flight dynamic characteristics of the F-106B configuration with vortex flaps. This report presents results of longitudinal and lateral-directional stability and control characteristics from static force tests, dynamic forced-oscillation tests, and free-flight tests on a 0.15-scale model of the F-106B airplane with vortex flaps. Highlights of this investigation were presented in reference 10; however, more detailed information is presented herein.

Symbols

All longitudinal forces and moments are referred to the wind axis system, and all lateral-directional forces and moments are referred to the body axis system. Airplane aerodynamic moments are referred to a moment reference center located longitudinally at $0.275\bar{c}$, which corresponds to a nominal mid center-of-gravity location for the airplane (fig. 4).

b	wing span, ft
C_D	drag coefficient, $\frac{\text{Drag}}{q_\infty S}$
C_L	lift coefficient, $\frac{\text{Lift}}{q_\infty S}$
C_l	rolling-moment coefficient, $\frac{\text{Rolling moment}}{q_\infty S b}$
ΔC_l	incremental rolling-moment coefficient due to control deflections
C_m	pitching-moment coefficient, $\frac{\text{Pitching moment}}{q_\infty S \bar{c}}$
C_n	yawing-moment coefficient, $\frac{\text{Yawing moment}}{q_\infty S b}$
ΔC_n	incremental yawing-moment coefficient due to control deflections
C_Y	side-force coefficient, $\frac{\text{Side force}}{q_\infty S}$
$\bar{c}$	mean aerodynamic chord, ft
FS	fuselage station, in.
I_X, I_Y, I_Z	moment of inertia about x-, y-, or z-axis, respectively
k	reduced-frequency parameter, $\frac{\omega b}{2V_\infty}$
p	roll rate, rad/sec
q	pitch rate, rad/sec
q_∞	free-stream dynamic pressure, lb/ft^2
r	yaw rate, rad/sec
s	Laplace operator
S	wing reference area, ft^2
V_∞	free-stream velocity, ft/sec
WL	waterline, in.
α	angle of attack, deg

$\dot{\alpha}$	rate of change of α, rad/sec
β	angle of sideslip, deg
$\dot{\beta}$	rate of change of β, rad/sec
δ_a	effective aileron deflection $(\delta_{ev,R} - \delta_{ev,L})/2$, deg
δ_e	effective elevator deflection, $(\delta_{ev,R} + \delta_{ev,L})/2$, deg
δ_{ev}	elevon deflection, positive trailing edge down, deg
$\delta_{f,le}$	leading-edge flap deflection, measured normal to flap hinge line and with respect to wing chord plane, positive leading edge down, deg
δ_r	rudder deflection, positive trailing edge left, deg
ω	angular velocity, rad/sec

Subscripts:

L	left
R	right

Derivatives:

$$C_{n_{\beta,\mathrm{dyn}}} = C_{n_\beta} \cos\alpha - \frac{I_Z}{I_X} C_{l_\beta} \sin\alpha$$

$$C_{l_\beta} = \frac{\partial C_l}{\partial \beta} \quad C_{n_\beta} = \frac{\partial C_n}{\partial \beta} \quad C_{Y_\beta} = \frac{\partial C_Y}{\partial \beta}$$

$$C_{l_p} = \frac{\partial C_l}{\partial \frac{pb}{2V}} \quad C_{n_p} = \frac{\partial C_n}{\partial \frac{pb}{2V}} \quad C_{Y_p} = \frac{\partial C_Y}{\partial \frac{pb}{2V}}$$

$$C_{l_{\dot{\beta}}} = \frac{\partial C_l}{\partial \frac{\dot{\beta}b}{2V}} \quad C_{n_{\dot{\beta}}} = \frac{\partial C_n}{\partial \frac{\dot{\beta}b}{2V}} \quad C_{Y_{\dot{\beta}}} = \frac{\partial C_Y}{\partial \frac{\dot{\beta}b}{2V}}$$

$$C_{l_r} = \frac{\partial C_l}{\partial \frac{rb}{2V}} \quad C_{n_r} = \frac{\partial C_n}{\partial \frac{rb}{2V}} \quad C_{Y_r} = \frac{\partial C_Y}{\partial \frac{rb}{2V}}$$

$$C_{N_q} = \frac{\partial C_N}{\partial \frac{q\bar{c}}{2V}} \quad C_{m_q} = \frac{\partial C_m}{\partial \frac{q\bar{c}}{2V}}$$

$$C_{N_{\dot{\alpha}}} = \frac{\partial C_N}{\partial \frac{\dot{\alpha}\bar{c}}{2V}} \quad C_{m_{\dot{\alpha}}} = \frac{\partial C_m}{\partial \frac{\dot{\alpha}\bar{c}}{2V}}$$

Model and Tests

Vortex Flap Designs

Three vortex flap configurations, illustrated in figure 5, were investigated. The full-span and part-span gothic vortex flaps were analytically designed for the F-106B airplane by the method of reference 4. The description and testing of these designs are discussed in more detail in reference 9. The other vortex flap configuration, the full-span constant-chord configuration, was a modification to the gothic vortex flap design in the apex area as a result of flow visualization tests on the full-scale semispan model (ref. 10).

The analytical design procedure for vortex flaps is based on the assumption that the most efficient flap condition for drag reduction is obtained when vortex flow reattachment occurs along the flap hinge line and the vortex flow is contained within the flap area. The design conditions for the vortex flap were a maneuver lift coefficient of 0.5 at a Mach number of 0.3 and a leading-edge deflection of 30° (measured normal to the hinge line). For this investigation, only vortex flap designs that attached to the existing wing leading edge were investigated. Thus, the wing leading edge became the flap hinge line on the F-106B vortex flap configuration.

The full-span constant-chord vortex flap was a result of flow observations that showed an unstable vortex formation in the apex area of the analytically designed gothic flap (ref. 10). A constant-sweep, finite-chord modification in the flap apex area was used to stabilize the formation of vortex flow onto the flap. The modified flap tested in this investigation was fabricated simply as a constant-chord flap with a finite-chord apex region.

Model Description

The geometric characteristics of the basic F-106B configuration are depicted in the three-view sketch of figure 4. A photograph of the 0.15-scale free-flight model is shown in figure 6. The model was constructed such that geometric and mass properties were scaled to represent the basic F-106B airplane for the purpose of determining flight characteristics from free-flight tests in the Langley 30- by 60-Foot Tunnel. Geometric and mass characteristics of the model are shown in table I. Elevon control surfaces located at the trailing-edge area of the wing actuate both elevator and aileron controls for the airplane. Ailerons were deflected differentially an equal amount relative to the elevator deflection; that is, if $\delta_{a,L} = -7°$, $\delta_{a,R} = 7°$, and $\delta_e = -10°$, then the left elevon would be deflected 17° trailing edge up while the right elevon would be deflected 3° trailing

edge up. For tests with vortex flaps installed, the leading-edge notch of the basic wing was sealed and faired.

Tests

The free-flight test technique is illustrated in figure 7 and described in reference 11. In such tests, powered, instrumented, dynamically scaled models are flown by remote control in level flight up to stall departure to investigate stability and control characteristics and to identify any tendencies of models to depart from controlled flight. The free-flight control system, depicted in figure 8, incorporates high performance electropneumatic actuators and a minicomputer to simulate the flight control system for a given configuration. Diagrams of the control laws used on the free-flight model are presented in figure 9. In each axis, pilot stick and trim inputs were combined with the stability augmentation system (SAS) signals. The SAS is comprised of angular rate feedbacks about each of the three body axes. The rate damper signals used in the control laws are provided by a three-axis gyro package and can be independently switched on or off about each axis. Test results are typically in the form of pilot comments, movies, and time histories of flight motions. For the free-flight tests, the vortex flap tested was the full-span gothic flap installed at a deflection angle of 50°.

Static force tests were conducted at a nominal free-stream dynamic pressure of 4.0 lb/ft^2, which corresponds to a Reynolds number based on the mean aerodynamic chord of 1.3×10^6. This Reynolds number was similar to that for the free-flight tests. Angle of attack ranged from $-4°$ to 50°, and angle of sideslip ranged from $-20°$ to 20°. The vortex flaps were tested at deflection angles of 30°, 40°, and 50° relative to the wing chord plane and normal to the wing leading edge.

Dynamic forced-oscillation tests were made about the roll, yaw, and pitch axes. The forced-oscillation test technique is described in reference 12. A photograph of the free-flight model installed on the oscillation rig in the 30- by 60-Foot Tunnel is shown in figure 10. Data were obtained for the vortex flap configurations with a deflection angle of 50° at an oscillation reduced-frequency parameter k of 0.20 about an angular amplitude of ±5°.

Results and Discussion

The results of static force tests, dynamic forced-oscillation tests, and free-flight tests are discussed in the following sections. Static force tests and dynamic forced-oscillation tests provide aerodynamic data for analysis of flight characteristics of the F-106B configuration with vortex flaps. Model free-flight tests are conducted in the 30- by 60-Foot Tunnel to evaluate, with the aid of static and dynamic test data, potential problem areas in flight.

Static Force Tests

Static longitudinal aerodynamic characteristics. The effect of deflecting the various vortex flaps on the longitudinal aerodynamic characteristics is shown by the data of figure 11. Data for the basic configuration without vortex flaps were also plotted for comparison purposes. In general, the lift and pitching-moment data are fairly linear up to $\alpha = 24°$. The lift curves indicate that the vortex flap configurations exhibited higher maximum values of C_L, primarily due to the increased wing planform area from the addition of the vortex flaps to the basic leading edge of the wing. In the range of angle of attack where the pitching-moment data are linear, the longitudinal stability is reduced, primarily because of the addition of the vortex flap area and the redistribution of vortex action on the flap; however, stability changes due to leading-edge deflection angle were not significant. The addition of the full-span gothic flap, the full-span constant-chord flap, and the part-span flap reduced the longitudinal positive static margin $-\frac{\partial C_m}{\partial C_L}$ from about 7 percent for the basic configuration to about 3 percent for the full-span flaps and 4 percent for the part-span flap. The reduction in static margin for the part-span flap was less than that for the full-span flaps because of the difference in flap area on the inboard 25-percent region of the span.

Figure 12 shows the effect of elevator deflection on the longitudinal aerodynamic characteristics of the full-span constant-chord configuration with various leading-edge deflections. Also shown in figure 12(a) for comparison are the data for the effect of elevator deflection on the basic configuration. The data of figure 12 indicate that control effectiveness of the vortex flap configuration was generally similar to that of the basic configuration. A comparison of the pitching-moment values for the various leading-edge flap deflections shown in figures 12(b), 12(c), and 12(d) indicates that control power was generally similar for all three configurations, and therefore the leading-edge deflection angle did not significantly influence the control power of the elevator. However, because of the reduced static margin of the vortex flap configurations, smaller deflections of the elevator would be required to trim the vortex flap configuration for a given C_L. Also, since negative elevator deflections produce decrements of lift, the reduced static margin would allow for increased trimmed $C_{L,\max}$ values on the vortex flap configuration.

Static lateral aerodynamic characteristics. The lateral-directional stability characteristics C_{Y_β}, C_{n_β}, and C_{l_β} were obtained from the incremental forces and moments measured at $\beta = -4°$ and $\beta = 4°$. Figure 13 shows the effect of leading-edge flap deflection on the lateral-directional stability characteristics of the various vortex flap configurations. Data for the basic configuration are also plotted for comparison purposes. On the basic configuration, the directional stability C_{n_β} decreases with increasing angle of attack and becomes unstable at about $\alpha = 26°$. The dihedral effect $-C_{l_\beta}$ of the basic configuration becomes more stable with increasing angle of attack until about $\alpha = 22°$ where the dihedral effect starts to decrease and goes unstable at about $\alpha = 29°$. In the high angle-of-attack range where the lateral-directional characteristics of the basic configuration are unstable, the general effect of increasing leading-edge flap deflection is to provide increased lateral-directional stability of the configuration. The increase in lateral-directional stability contributes to improved yaw departure characteristics as indicated by the plot of the yaw divergence parameter $C_{n_{\beta,\mathrm{dyn}}}$ shown in figure 14. The parameter $C_{n_{\beta,\mathrm{dyn}}}$ incorporates the static lateral-directional stability derivatives C_{n_β} and C_{l_β} to represent the directional stability characteristics under dynamic conditions. The parameter has been a good indicator of the angle of attack for yaw departure in previous free-flight investigations. The data of figure 14 indicate that the basic configuration exhibited stable values of $C_{n_{\beta,\mathrm{dyn}}}$ up to about $\alpha = 28°$, whereas the full-span gothic flap configuration extended the range of angle of attack where $C_{n_{\beta,\mathrm{dyn}}}$ was stable by several degrees.

The effect of elevator deflection on the lateral-directional stability characteristics is shown by the data of figure 15 for several leading-edge deflections of the full-span constant-chord flap configuration. Data for the basic configuration are also plotted for comparison. Generally, increasing elevator deflection trailing edge up has a destabilizing effect on directional stability C_{n_β} in the angle-of-attack range up to 30° and a stabilizing effect on the dihedral effect $-C_{l_\beta}$ in the angle-of-attack range from 28° to 40°.

The effect of the full-span constant-chord vortex flap on the directional stability provided by the vertical tail is shown in figure 16. The vertical tail provides a directional stability contribution up to about $\alpha = 34°$ on the basic configuration and up to about $\alpha = 39°$ on the vortex flap configuration. The favorable effect of the vortex flaps on the C_{n_β} contribution to the vertical tail is attributed to the improved flow field at the vertical tail location for the vortex flap configuration. As seen in other studies, the vortex flap may have delayed vortex bursting to a higher angle of attack and would thereby provide improved flow conditions for directional stability.

The control power of the aileron is shown by the data of figure 17 for the basic configuration and for the model with various deflections of the full-span constant-chord flap. Generally, the results indicate that roll control power up to $\alpha = 30°$ was not significantly affected by vortex flaps. For the model with elevators undeflected, roll control power was generally increased by the addition of vortex flaps above $\alpha = 30°$. Also, yawing moments due to aileron deflections are favorable for the model with or without the vortex flaps.

The effect of various deflections of the full-span constant-chord flap on rudder control power is shown by the data of figure 18. Data for the basic configuration are also shown for comparison purposes. Generally, vortex flaps did not significantly affect the rudder control power below $\alpha = 35°$. However, the vortex flaps reduced the directional control above $\alpha = 35°$.

Dynamic Forced-Oscillation Tests

Damping characteristics obtained from dynamic forced-oscillation tests about the roll, yaw, and pitch axes are shown in figures 19 through 21. A potential concern about the vortex flap configurations was the possibility that the flap vortex would move off the flap surface as the airplane is oscillated in roll, and thereby influence the dynamic damping characteristics of the airplane. The data of figure 19 indicate that the basic configuration exhibited stable roll damping characteristics throughout the test angle-of-attack range. The addition of the full-span gothic flap provided only small changes to the roll damping characteristics up to $\alpha = 30°$. Above $\alpha = 30°$, the gothic flap reduced the roll damping for some angles of attack but the damping remained stable throughout the test angle-of-attack range. The yaw damping characteristics, shown in figure 20, indicate that the basic configuration exhibited stable characteristics throughout the test angle-of-attack range, whereas the vortex flaps reduced yaw damping above $\alpha = 20°$ and caused the yaw damping to become unstable at about $\alpha = 45°$. Pitch damping characteristics, shown in figure 21, indicate that vortex flaps had no significant effect below $\alpha = 30°$. The vortex flap configurations did exhibit unstable pitch damping at $\alpha = 35°$.

Free-Flight Tests

The 0.15-scale model was flown in the 30- by 60-Foot Tunnel, as shown in figure 22, to provide flight

characteristics for $1g$ level flight up to stall departure and to demonstrate and identify potential problem areas that may not be obvious in the aerodynamic data. The approach used in free-flight testing is to start out at a relatively low angle of attack and high tunnel free-stream velocity and gradually decrease tunnel velocity to obtain model flight characteristics at higher angle of attack. The model is then flown to its highest obtainable angle of attack for $1g$ flight before loss of control or stability problems cause the model to depart from controlled flight.

Longitudinal flight characteristics. The angle-of-attack range of the model free-flight tests is shown in figure 23. On both the basic configuration and the full-span gothic flap configuration, model flight tests were started at about $\alpha = 15°$. The basic model flew very steadily and was easy to fly with little pilot effort. The longitudinal motions were well damped and the response to control inputs was rapid. The longitudinal flight behavior remained very good as the angle of attack increased, although, as expected, the control response was not as rapid as it was at the higher speeds. Flights for the basic configuration were terminated at about $\alpha = 30°$ because of an uncontrollable yaw divergence.

The addition of the vortex flaps to the model degraded the longitudinal flight behavior, primarily by reducing the static margin (fig. 11). The data of figure 11(a) show that the addition of the flaps reduced the longitudinal static margin from about 7 percent for the basic configuration to about 3 percent for the full-span gothic flap configuration. The reduced static margin was very noticeable to the pitch pilot because the model was very sensitive to gust disturbances and control inputs. The model was difficult to fly smoothly and required considerable pilot effort compared with that for the basic configuration.

Flights of the model with full-span gothic flaps were also conducted with increased artificial pitch damping in an attempt to improve flight behavior. The results of the tests indicated that increased pitch damping was a satisfactory means of improving the longitudinal flight behavior of the model. With increased damping, the model was very steady in pitch and could be flown smoothly with little pilot effort. Flights were made up to about $\alpha = 35°$, where an uncontrollable yaw divergence occurred.

The full-span gothic flap configuration was also flown with the center of gravity shifted forward to provide increased static margin similar to that of the basic configuration. The flight behavior of the model with the forward center of gravity was improved considerably and was generally similar to that of the basic configuration. The longitudinal motions were well damped and the response to control inputs was good. The model could be flown smoothly with little pilot effort up to about $\alpha = 35°$, where an uncontrollable yaw divergence occurred.

Lateral-directional flight characteristics. The lateral-directional flight characteristics of the basic configuration were considered to be generally very good. The model was well damped and was laterally-directionally stable and responded rapidly to control inputs. As the angle of attack increased, the roll and yaw damping appeared to increase, and the model flights became very steady. This increase in damping characteristic was expected based on the measured damping data of figures 19 and 20. Smooth sustained flights were possible with very little pilot effort up to about $\alpha = 30°$, where an uncontrollable yaw divergence occurred. The ailerons, in addition to roll control, produced favorable yaw, as indicated in figure 17, and this favorable yaw made sustained flight possible with ailerons alone up to the angle of attack of yaw divergence. However, coordinated control provided the best flying conditions because rudder effectiveness was maintained up through the yaw departure angle of attack, and the model was controllable up to the point of yaw departure. The divergence angle of attack is in good agreement with that predicted by $C_{n_{\beta,\mathrm{dyn}}}$ shown in figure 14.

With the addition of the full-span gothic flap, the model exhibited lateral-directional flight characteristics generally similar to those of the basic configuration. The motions were well damped and the damping appeared to increase with increasing angle of attack as predicted in the measured damping data of figures 19 and 20. As a result of the increased damping, the model flights became much steadier, and smooth sustained flights were possible up to about $\alpha = 35°$ where flights were terminated by a yaw divergence. The yaw divergence angle of attack for the vortex flap configuration is about 2° higher than predicted by the $C_{n_{\beta,\mathrm{dyn}}}$ parameter of figure 14.

The lateral-directional control response appeared to be similar to that for the basic configuration. That is, ailerons alone provided adequate control up to about $\alpha = 32°$ and rudder effectiveness remained good up through the yaw departure angle of attack. Coordinated control provided the best flying condition and was used to maintain smooth sustained flights over the test angle-of-attack range. The fact that the model could be flown to $\alpha = 35°$ can probably be attributed to the effective lateral-directional controls (refer to figs. 17 and 18) which allowed the roll and yaw pilot to keep the model angular motions small and prevent large excursions from starting.

Summary of Results

An investigation to determine the effects of vortex flaps on the flight dynamic characteristics of the F-106B in the area of low-speed, high-angle-of-attack flight was undertaken on a 0.15-scale model of the airplane in the Langley 30- by 60-Foot Tunnel. Static force tests, dynamic forced-oscillation tests, and free-flight tests were conducted to obtain a data base on the flight characteristics of the F-106B airplane with vortex flaps. Vortex flap configurations tested included a full-span gothic flap, a full-span constant-chord flap, and a part-span gothic flap.

The major results of this investigation are summarized as follows:

1. Static force tests indicated that the addition of vortex flaps to the basic wing configuration caused the static longitudinal stability to be reduced from a static margin of 7 percent for the basic configuration at the nominal mid center-of-gravity location to about 3 percent for the full-span flap configurations and to about 4 percent for the part-span flap configuration. Longitudinal stability changes due to leading-edge deflection angles were small in comparison with those due to adding vortex flaps.

2. Vortex flaps provided the configuration with improved static lateral-directional stability at high angles of attack. The improved lateral-directional stability characteristic provided an increase in angle of attack at which the yaw divergence parameter $C_{n_{\beta,\mathrm{dyn}}}$ remained stable.

3. Dynamic forced-oscillation tests indicated that vortex flaps did not significantly affect the damping characteristics of the configuration about the roll, yaw, or pitch axes at angles of attack below 30°.

4. Free-flight tests with the full-span gothic flap indicated that the reduced static longitudinal stability degraded the flight characteristics of the model because of increased sensitivity to control inputs. A shift in center-of-gravity location to a forward position or an addition of artificial pitch damping with rate gyros resulted in good longitudinal flight behavior.

5. The model with the full-span gothic flap exhibited lateral-directional flight characteristics generally similar to those of the basic model. The motions were well damped and the damping appeared to increase with increasing angle of attack.

6. The basic configuration exhibited yaw departure at an angle of attack of about 30°. With the full-span gothic flap, the yaw departure angle of attack was increased to about 35°. These results are in good agreement with the analysis made with the $C_{n_{\beta,\mathrm{dyn}}}$ data derived from static force tests.

NASA Langley Research Center
Hampton, Virginia 23665-5225
March 27, 1987

References

1. Lamar, John E.: Subsonic Vortex-Flow Design Study for Slender Wings. *J. Aircr.*, vol. 15, no. 9, Sept. 1978, pp. 611-617.

2. Rao, Dhanvada M.: *Leading Edge Vortex-Flap Experiments on a 74 Deg. Delta Wing.* NASA CR-159161, 1979.

3. Yip, Long P.; and Murri, Daniel G.: *Effects of Vortex Flaps on the Low-Speed Aerodynamic Characteristics of an Arrow Wing.* NASA TP-1914, 1981.

4. Frink, Neal T.: *Concept for Designing Vortex Flap Geometries.* NASA TP-2233, 1983.

5. Erickson, Gary E.: Application of Free Vortex Sheet Theory to Slender Wings With Leading-Edge Vortex Flaps. AIAA-83-1813, July 1983.

6. Lamar, John E.; and Campbell, James F.: Vortex Flaps—Advanced Control Devices for Supercruise Fighters. *Aerosp. America*, vol. 22, no. 1, Jan. 1984, pp. 95–99.

7. Schoonover, W. Elliott, Jr.; Frink, Neal T.; Hallissy, James B.; and Yip, Long P.: Subsonic/Transonic Development of Vortex Flaps for Fighter Aircraft. *Langley Symposium on Aerodynamics*, Volume II, Sharon H. Stack, compiler, NASA CP-2398, 1986, pp. 163–178.

8. Campbell, James F.; Osborn, Russell F.; and Foughner, Jerome T., Jr., eds.: *Vortex Flow Aerodynamics.* 1986.
   Volume I, NASA CP-2416.
   Volume II, NASA CP-2417.
   Volume III, NASA CP-2418.

9. Hallissy, James B.; Frink, Neal T.; and Huffman, Jarrett K.: Aerodynamic Testing and Analysis of Vortex Flap Configurations for the 5-Percent Scale F-106B. *Vortex Flow Aerodynamics*, Volume II, James F. Campbell, Russell F. Osborn, and Jerome T. Foughner, Jr., eds., NASA CP-2417, 1986, pp. 227–248.

10. Yip, Long P.: Investigation of Vortex Flaps on the F-106B Airplane Configuration in the 30- by 60-Foot Wind Tunnel. *Vortex Flow Aerodynamics*, Volume II, James F. Campbell, Russell F. Osborn, and Jerome T. Foughner, Jr., eds., NASA CP-2417, 1986, pp. 201–226.

11. Chambers, Joseph R.; Bowman, James S., Jr.; and Malcolm, Gerald N.: Stall/Spin Test Techniques Used by NASA. *Stall/Spin Problems of Military Aircraft*, AGARD-CP-199, June 1976, pp. 13-1–13-12.

12. Chambers, Joseph R.; and Grafton, Sue B.: *Static and Dynamic Longitudinal Stability Derivatives of a Powered 1/9-Scale Model of a Tilt-Wing V/STOL Transport.* NASA TN D-3591, 1966.

Table I. Geometric and Mass Properties of Basic Configuration

Parameter	Full scale	0.15 scale
Wing area, ft^2	697.83	15.70
Span, ft	38.13	5.72
Mean aerodynamic chord, ft	23.75	3.56
Location of leading edge of $\bar{c}$, in.	FS 345.90	FS 51.89
Center of gravity:		
Longitudinal location, in.	FS 431.41	FS 64.71
Vertical location, in.	WL −7.78	WL −1.17
Wing chord plane elevation, in.	WL −16.00	WL −2.40
Moment of inertia:		
I_X, slug-ft^2	18 654	1.42
I_Y, slug-ft^2	180 151	13.68
I_Z, slug-ft^2	192 512	14.85

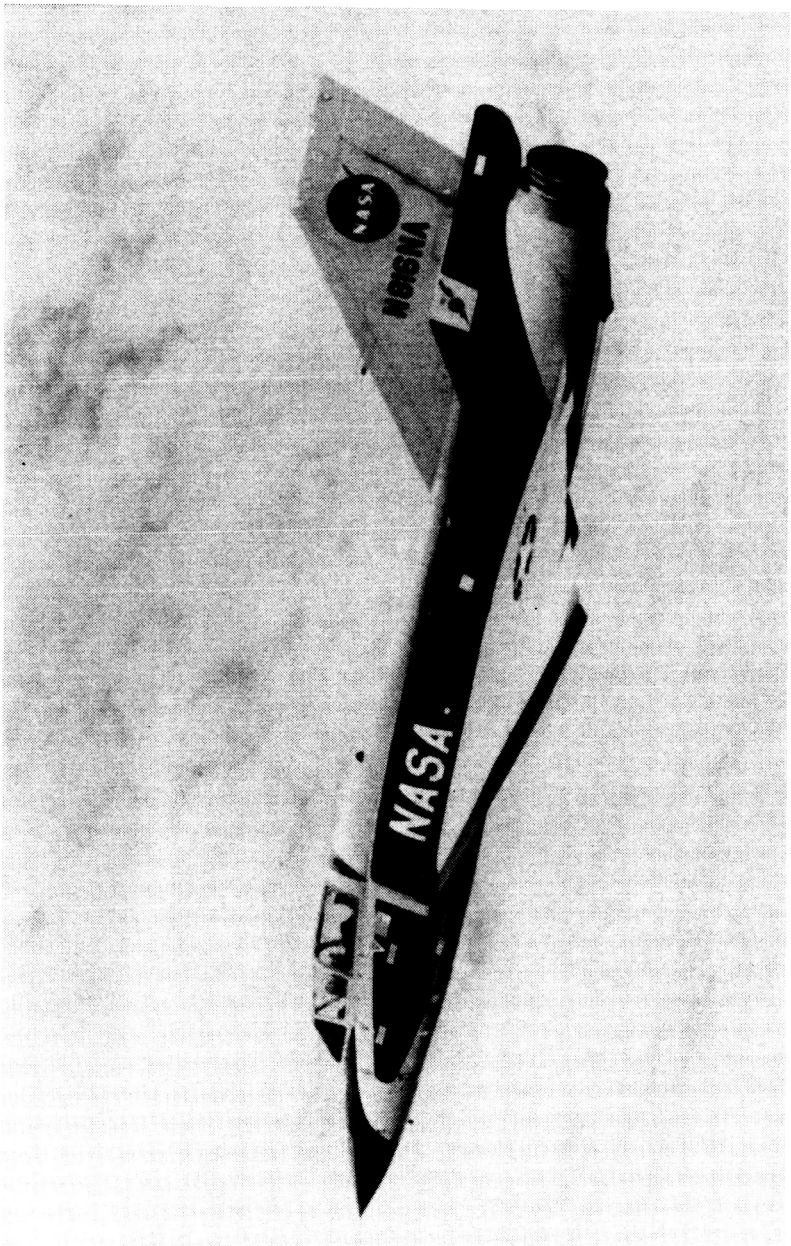

L-85-11,146

Figure 1. Artist's sketch of vortex flap on F-106B flight research airplane.

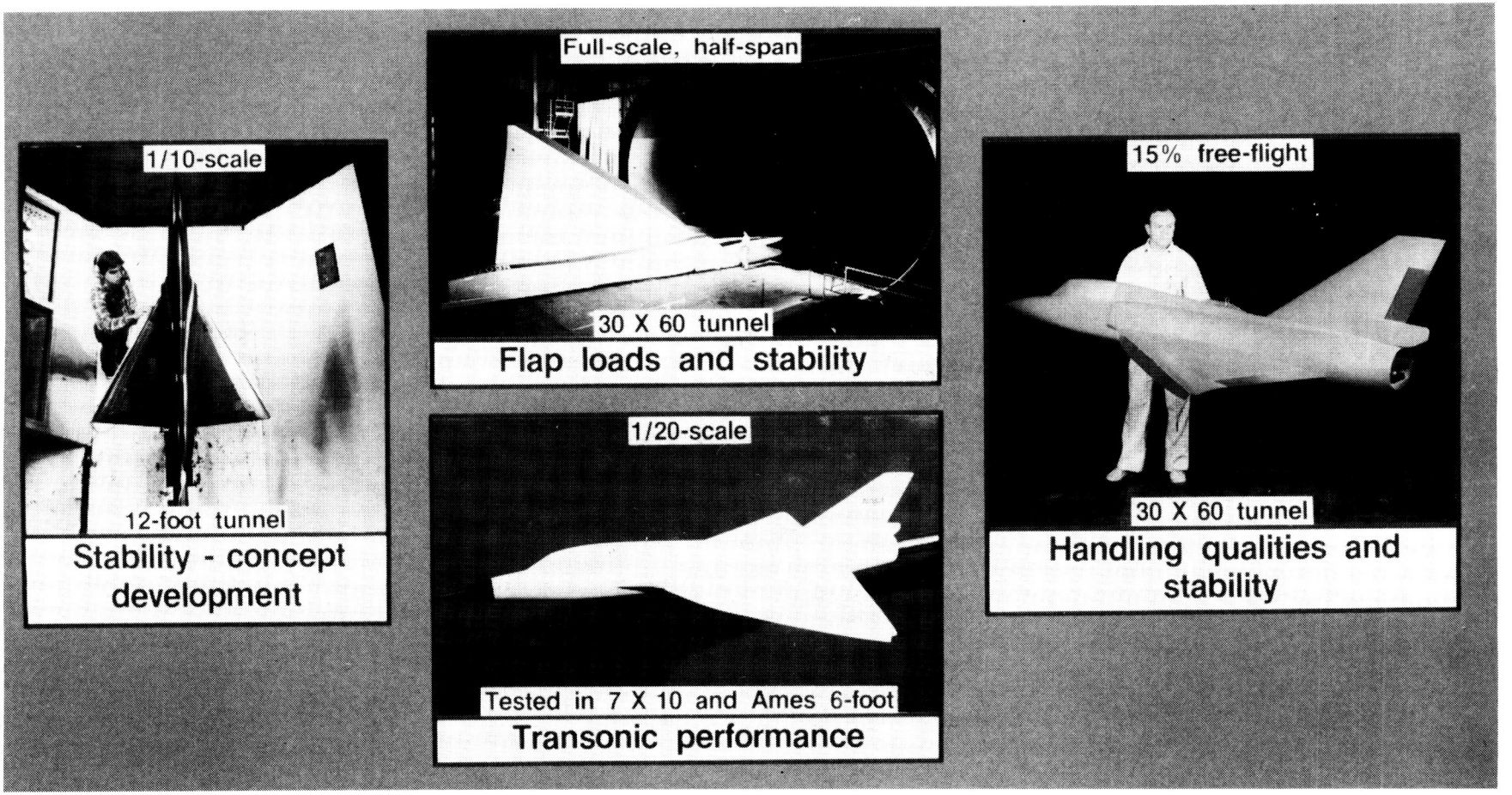

L-85-7722

Figure 2. Models of F-106B used in various vortex flap aerodynamic studies.

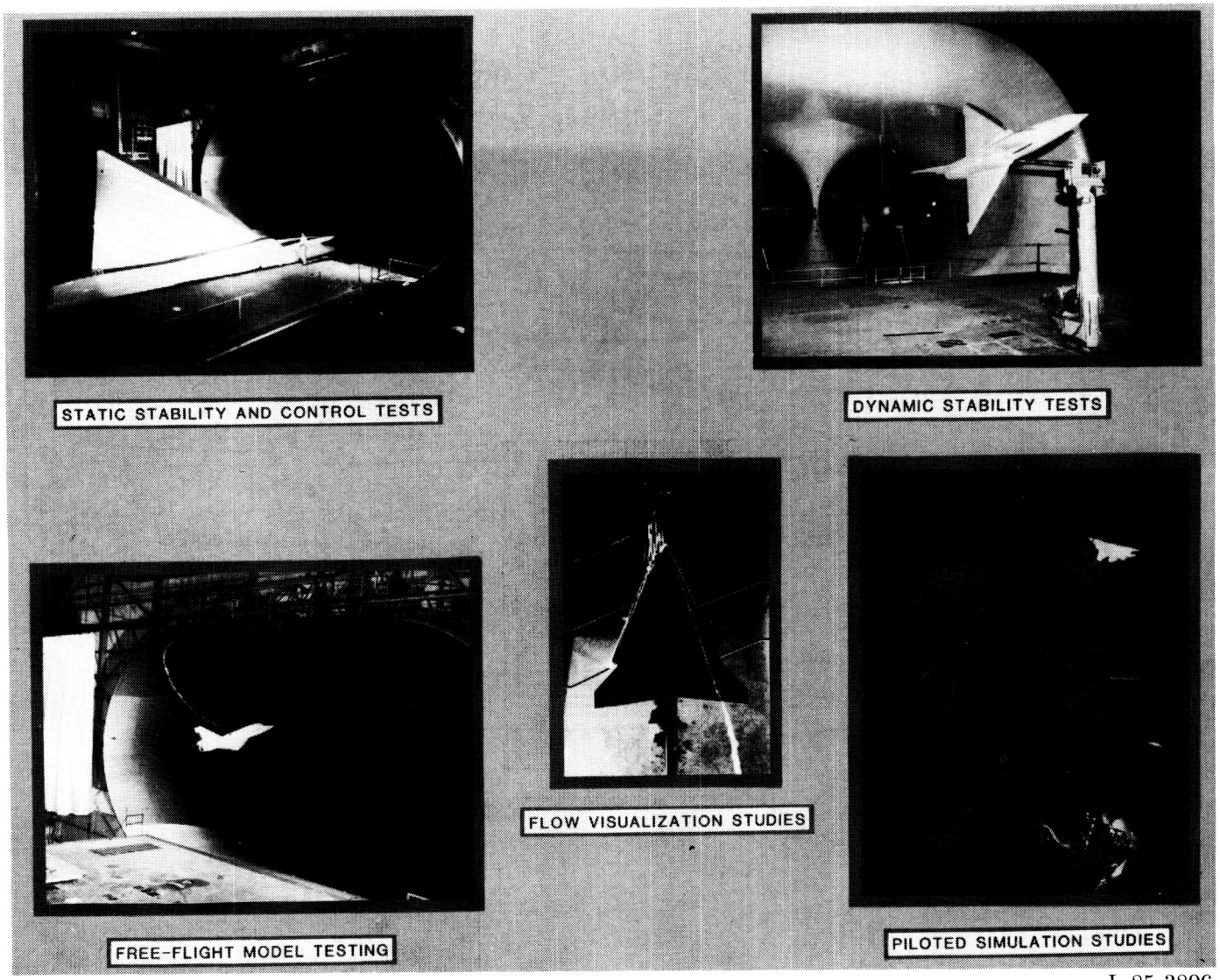

L-85-3806

Figure 3. Research approach used to study vortex flap aerodynamic characteristics in low-speed flight regime.

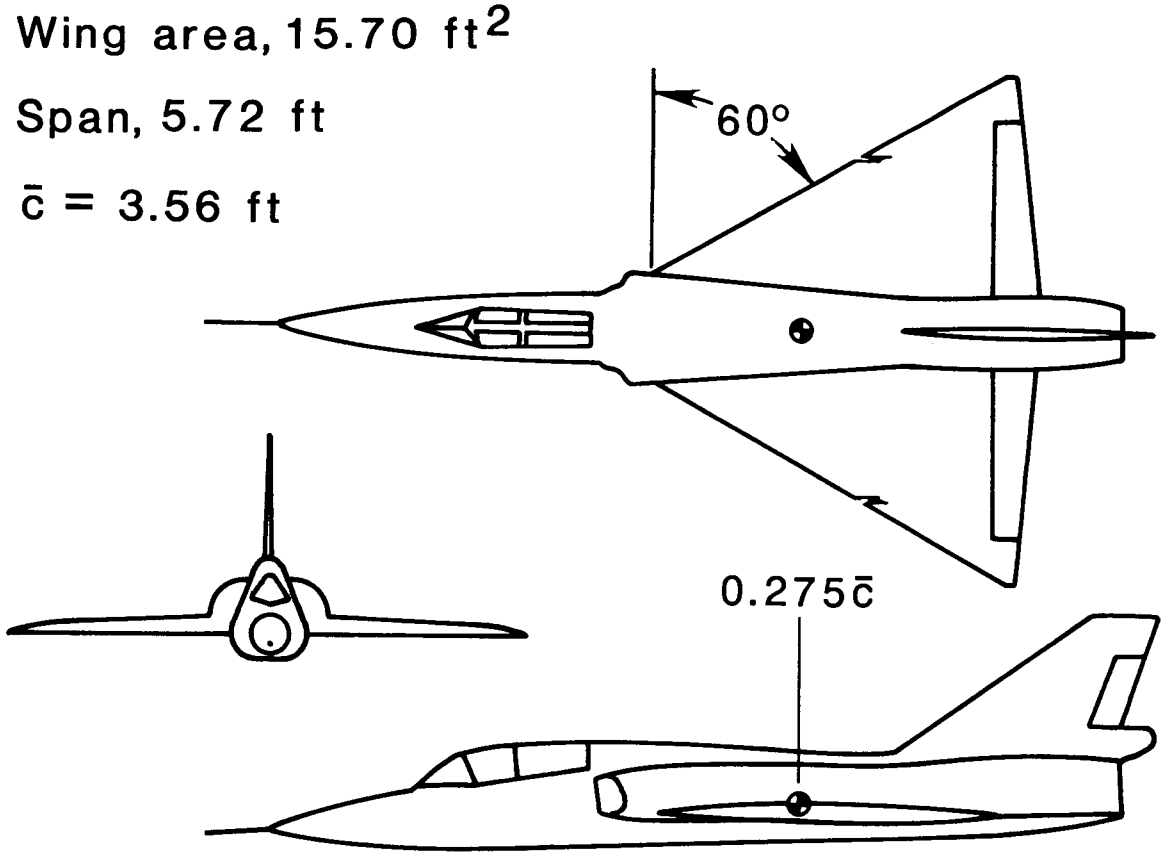

Figure 4. Basic F-106B configuration. Dimensions are for 0.15-scale model. Moment reference center is at $0.275\bar{c}$, which corresponds to nominal mid center-of-gravity location.

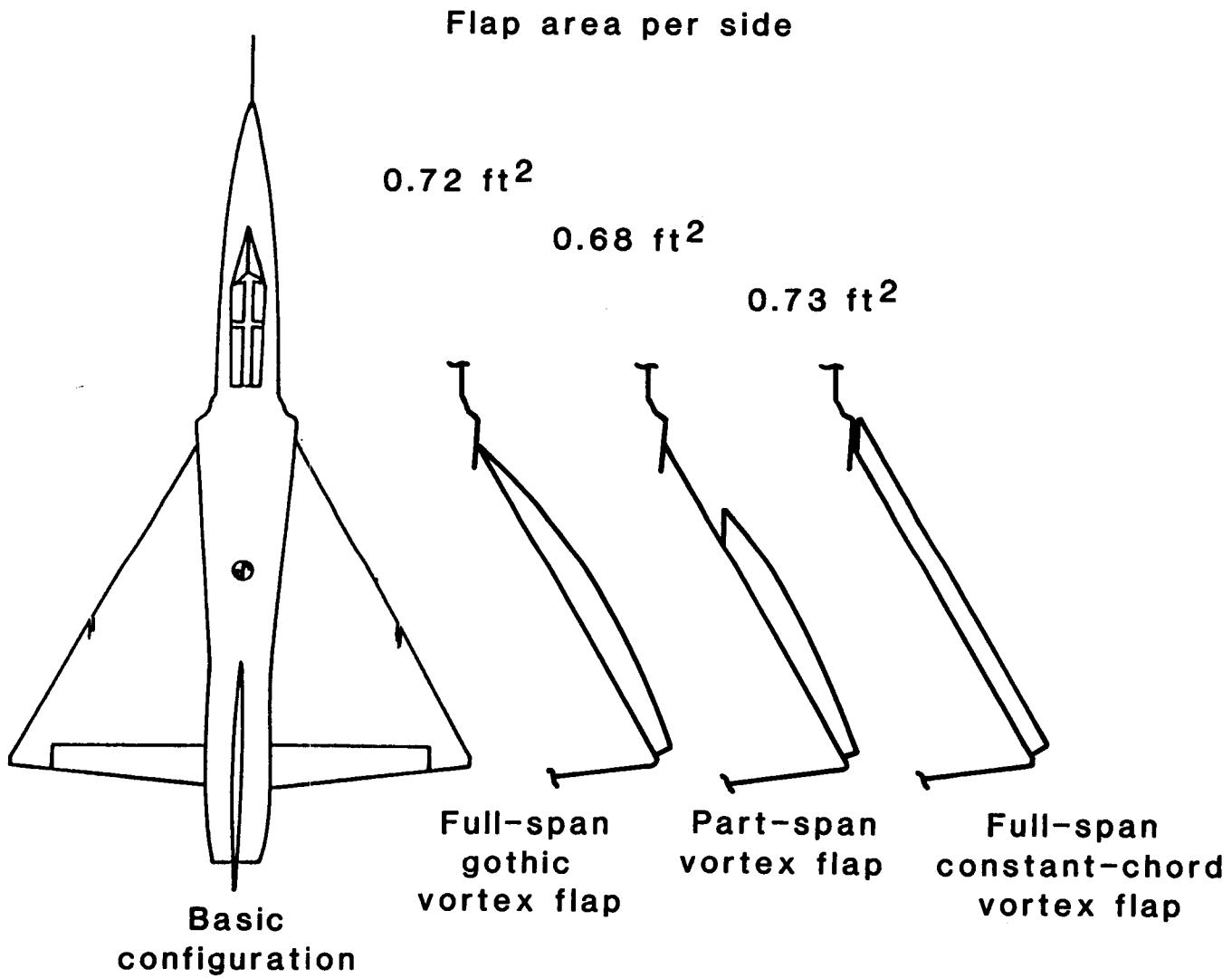

Figure 5. Vortex flap configurations tested.

L-84-6726

Figure 6. Three-quarter front view of 0.15-scale free-flight model of F-106B airplane with full-span gothic flaps.

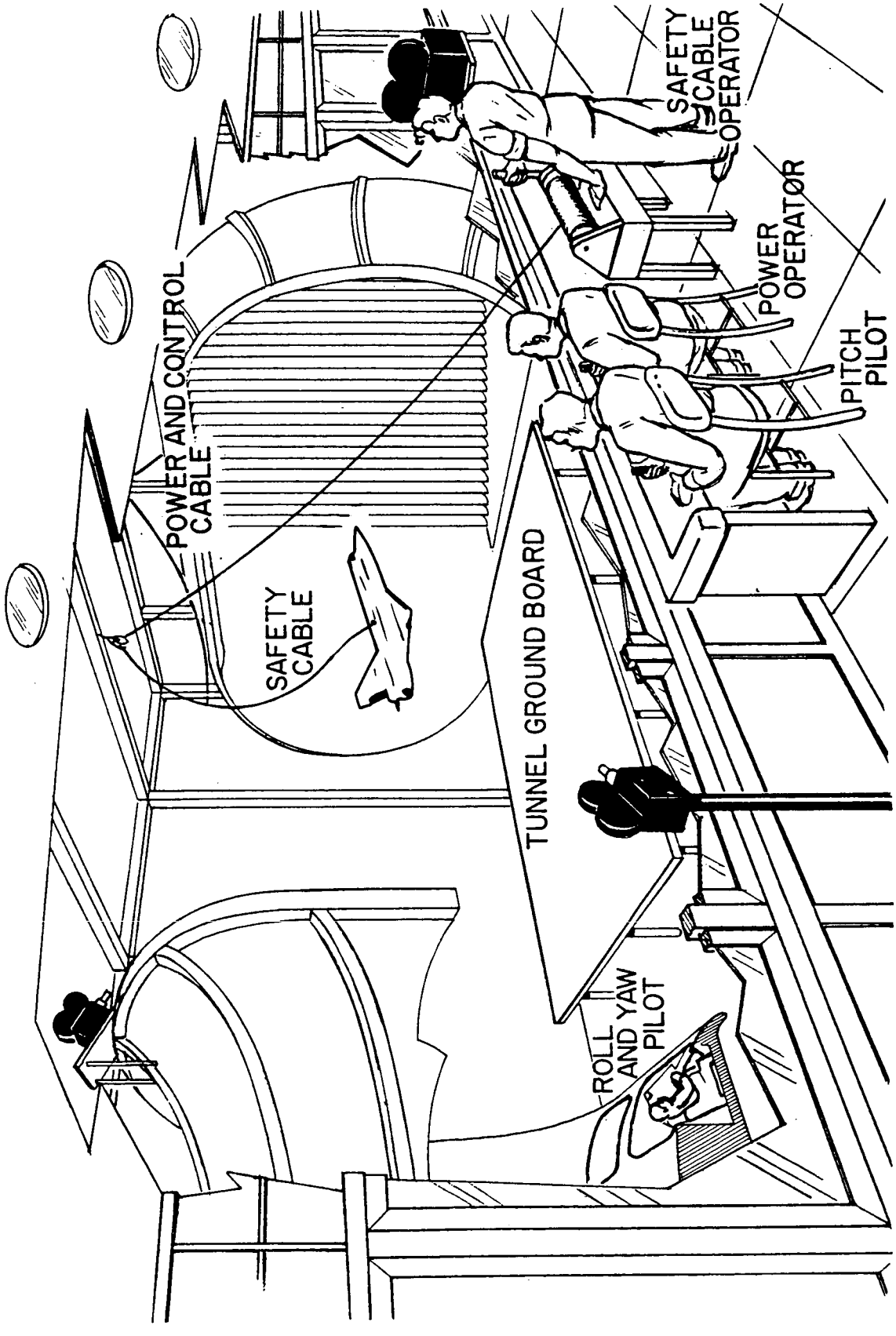

Figure 7. Free-flight test setup in Langley 30- by 60-Foot Tunnel.

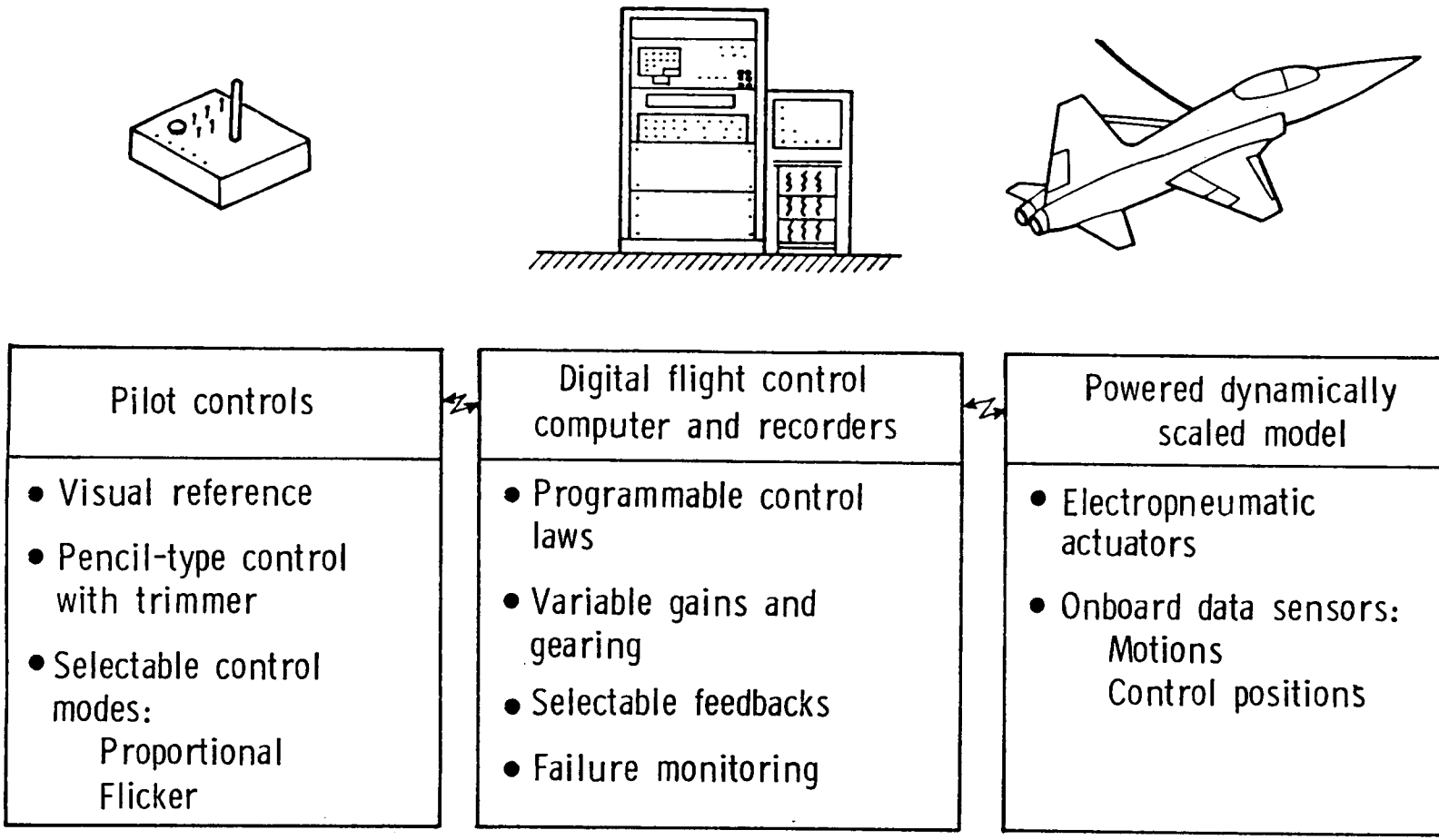

Figure 8. Free-flight model control system.

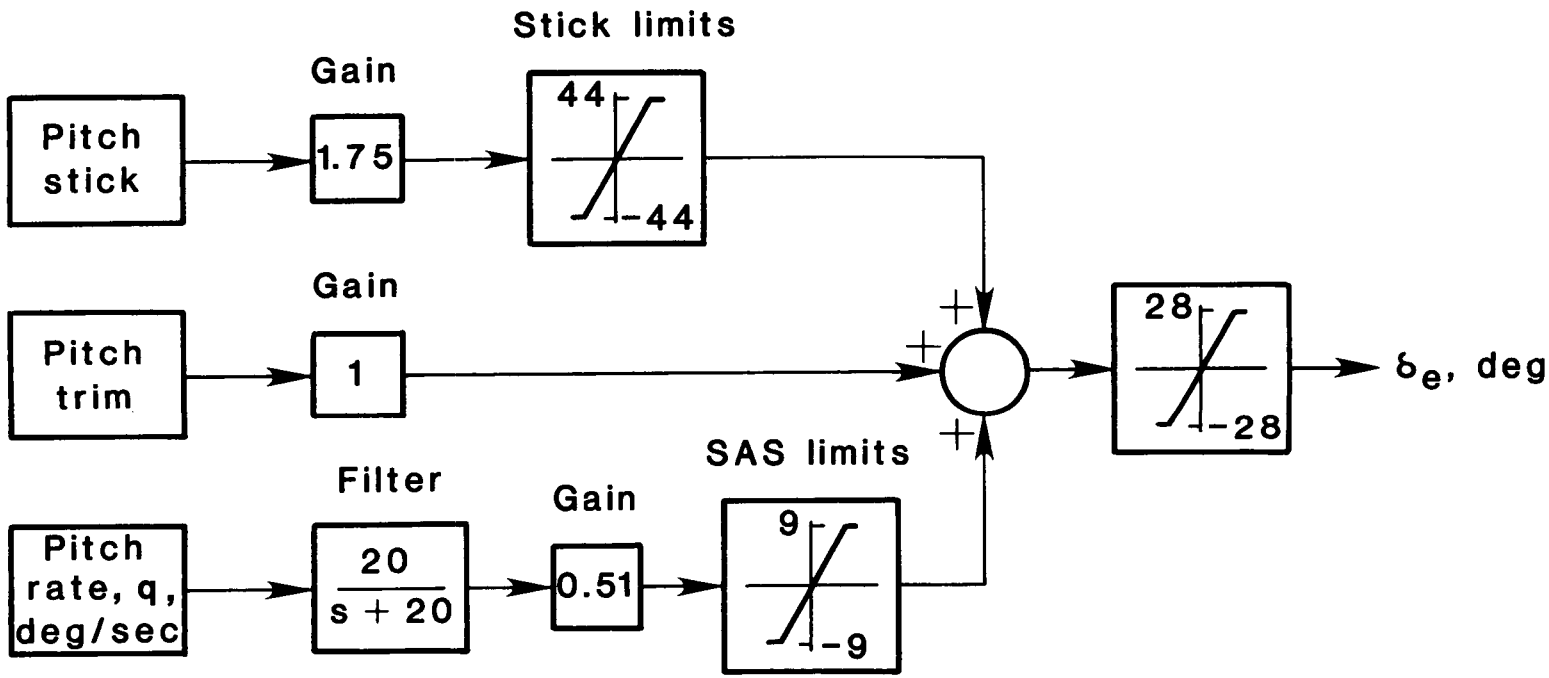

(a) Pitch.

Figure 9. Control laws used in free-flight tests.

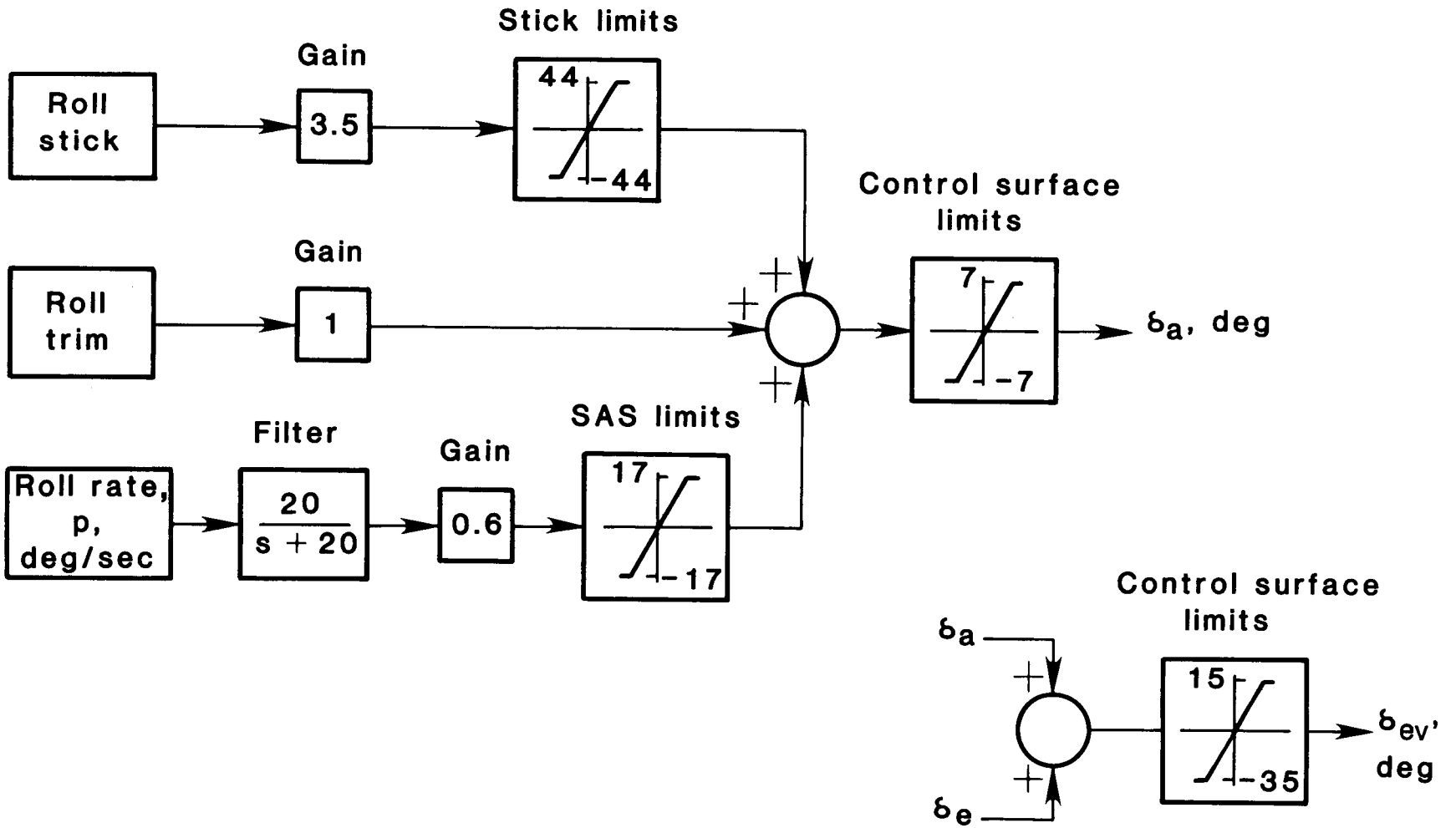

(b) Roll.

Figure 9. Continued.

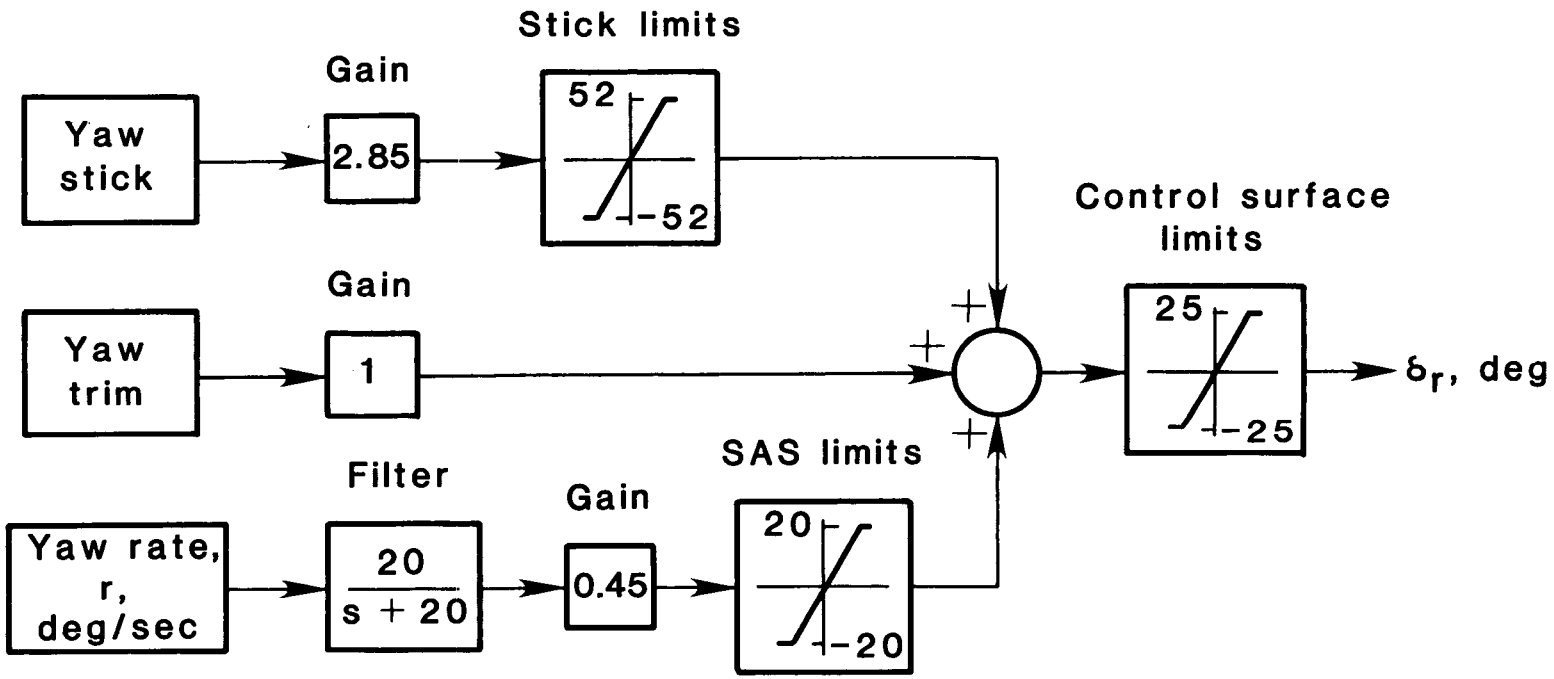

(c) Yaw.

Figure 9. Concluded.

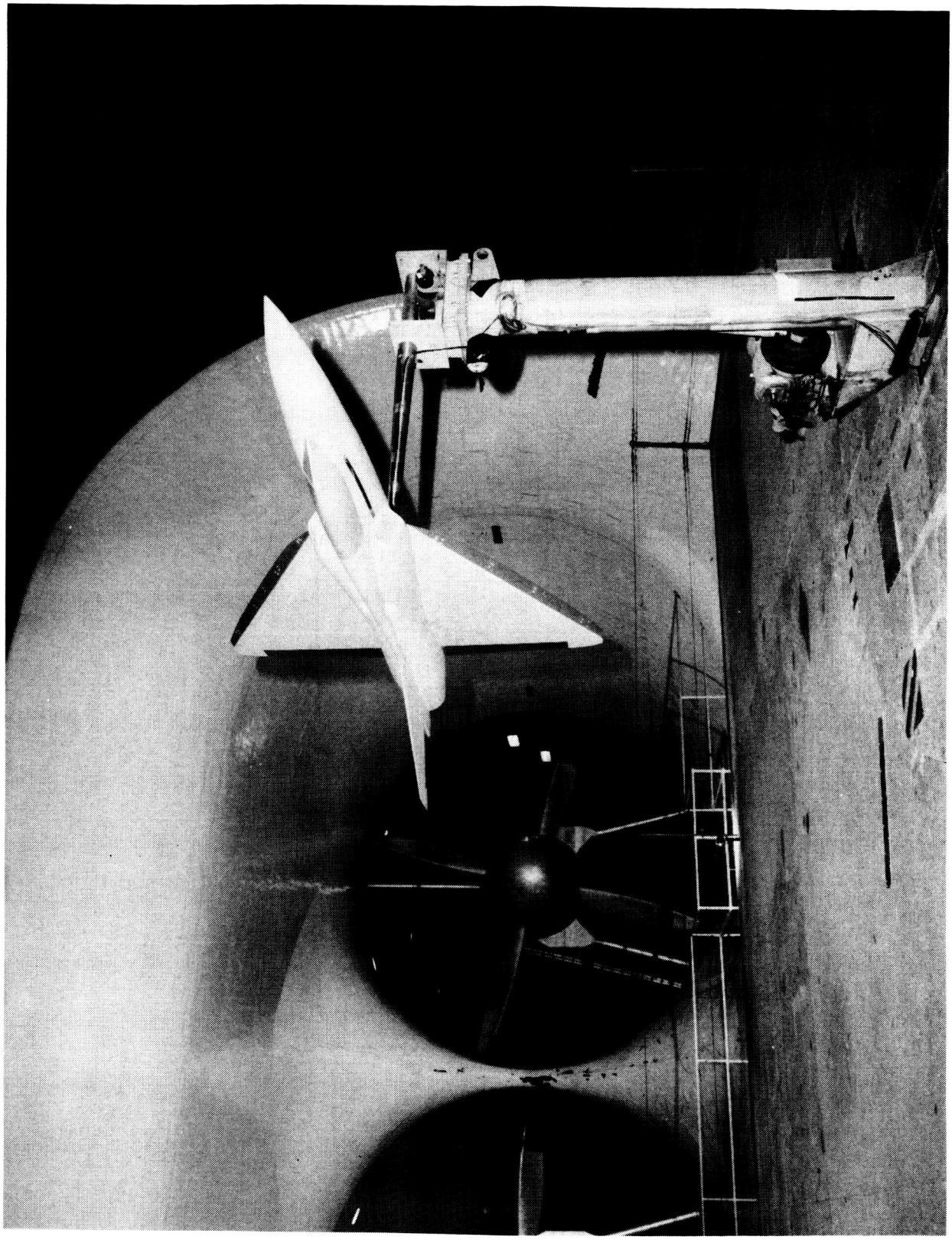

L-85-3183

Figure 10. Dynamic forced-oscillation test setup in Langley 30- by 60-Foot Tunnel.

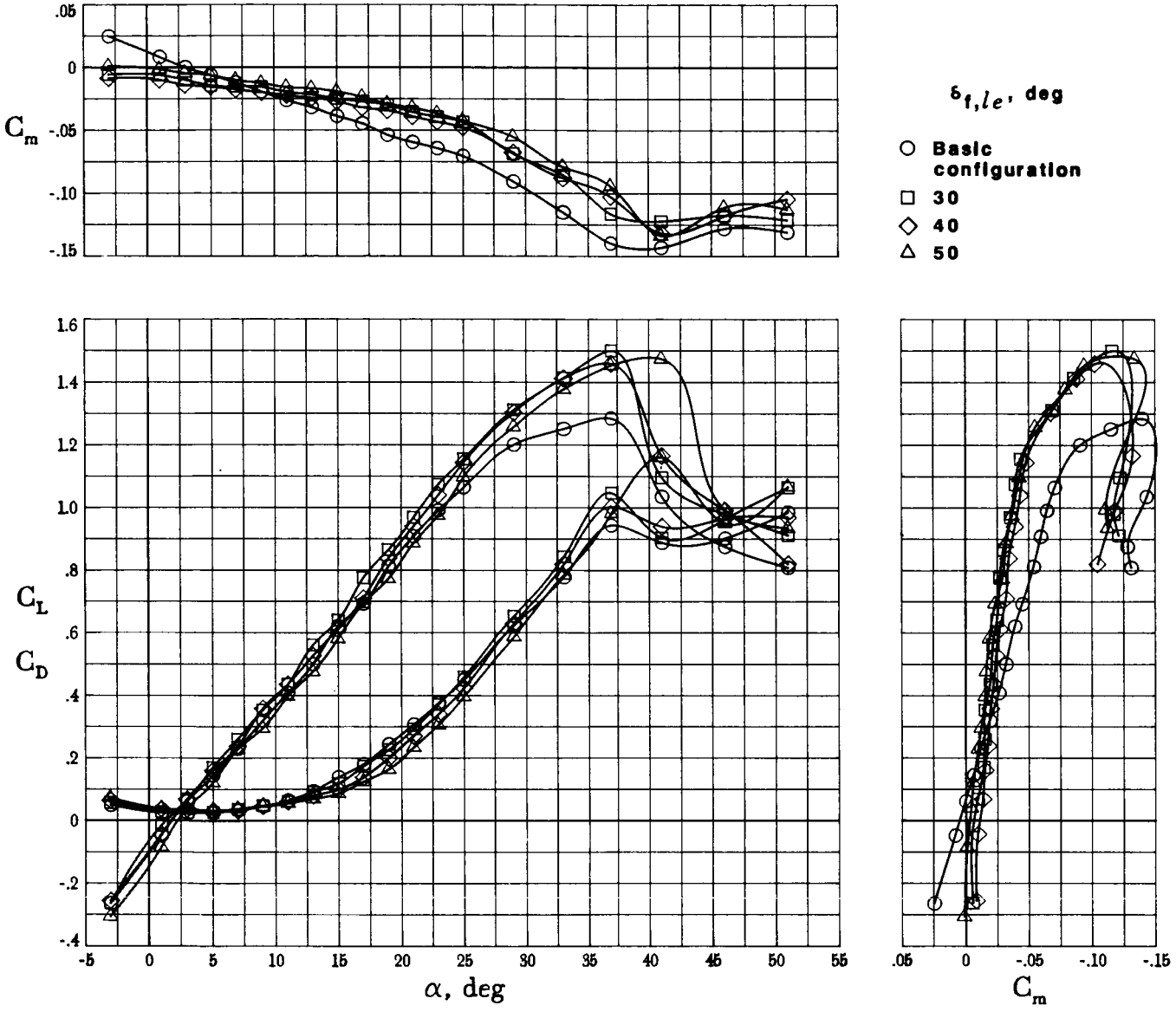

(a) Full-span gothic flap.

Figure 11. Effect of leading-edge flap deflection on longitudinal aerodynamic characteristics of various vortex flap configurations. $\delta_e = 0°$.

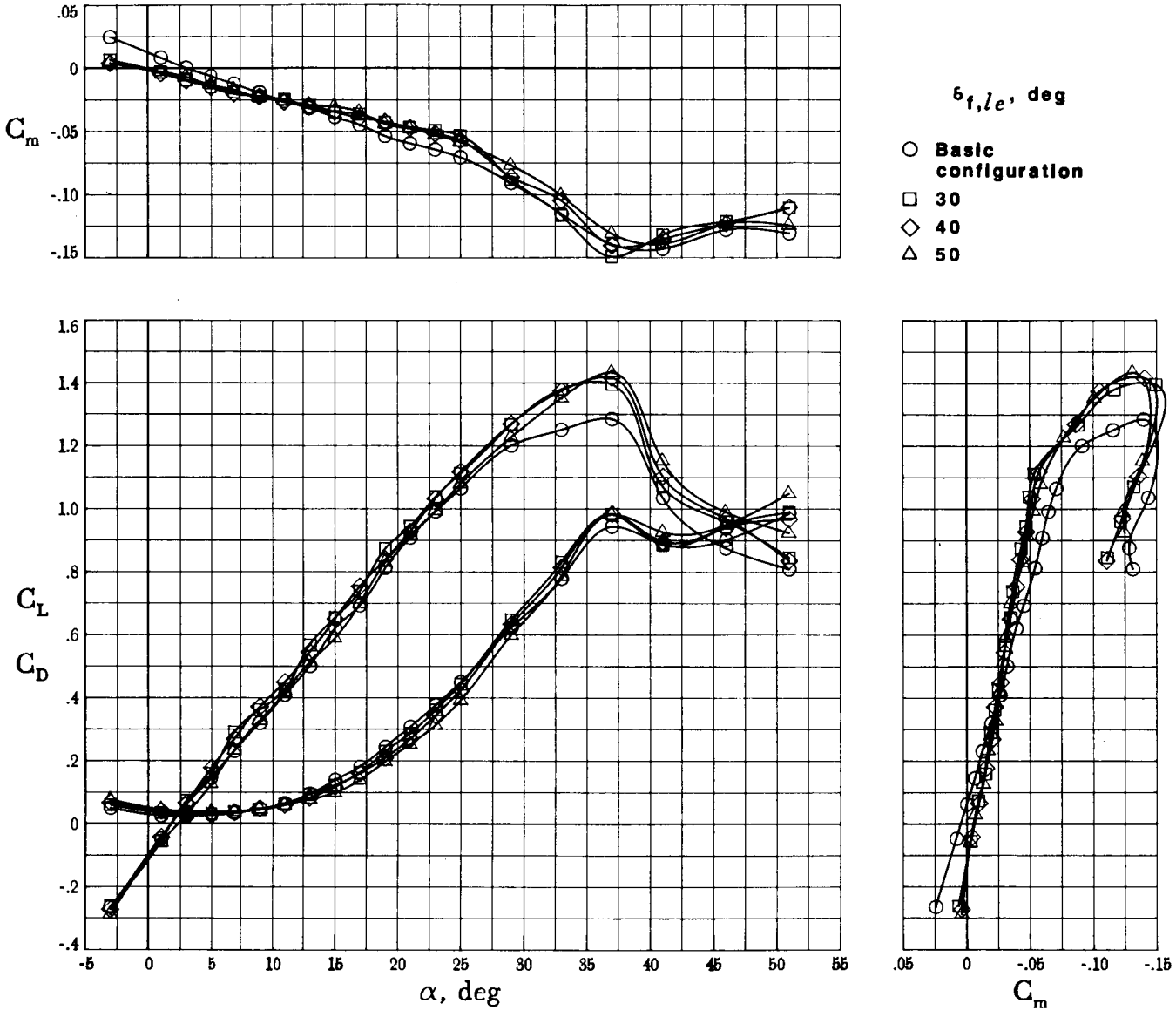

(b) Part-span flap.

Figure 11. Continued.

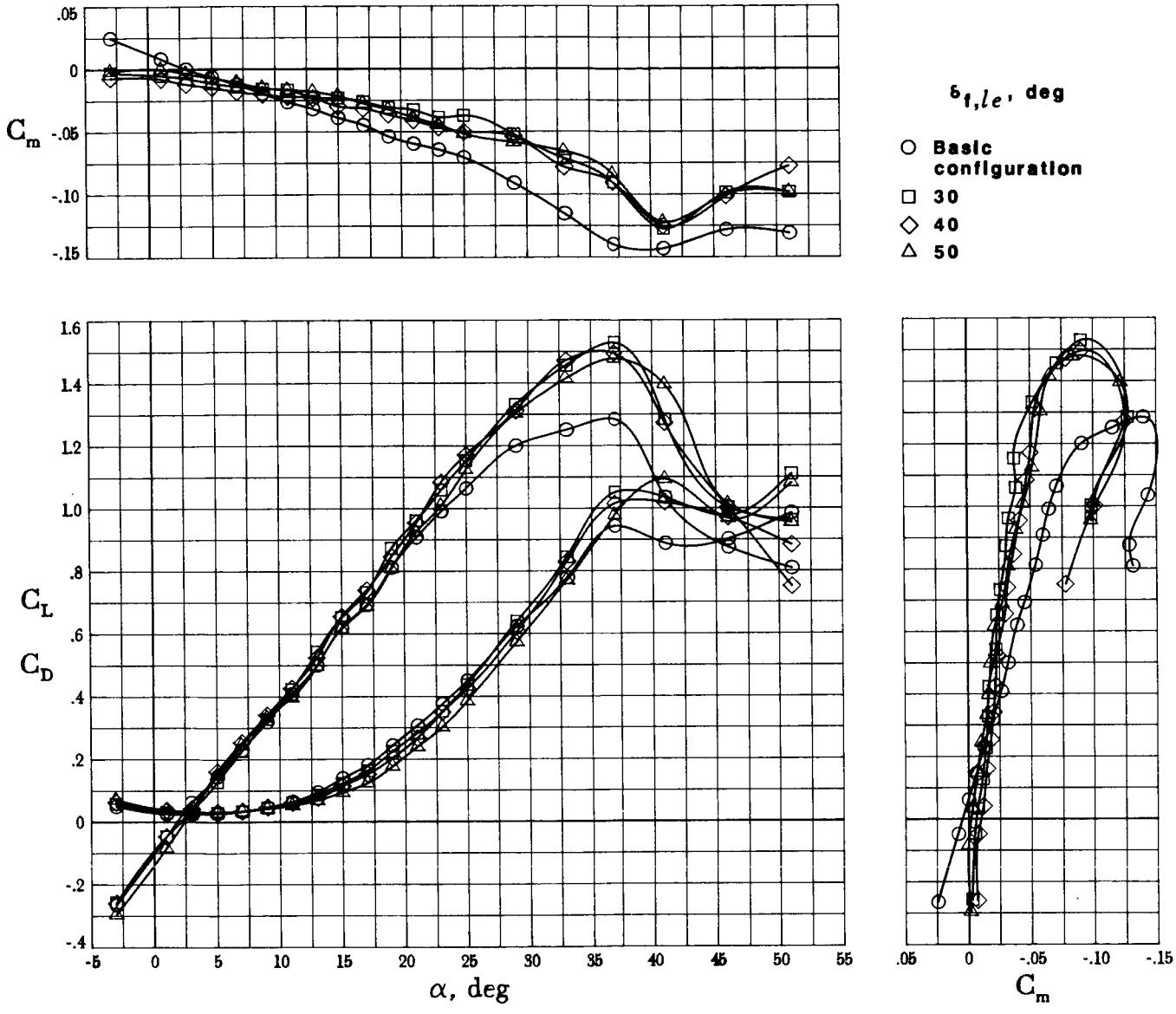

(c) Full-span constant-chord flap.

Figure 11. Concluded.

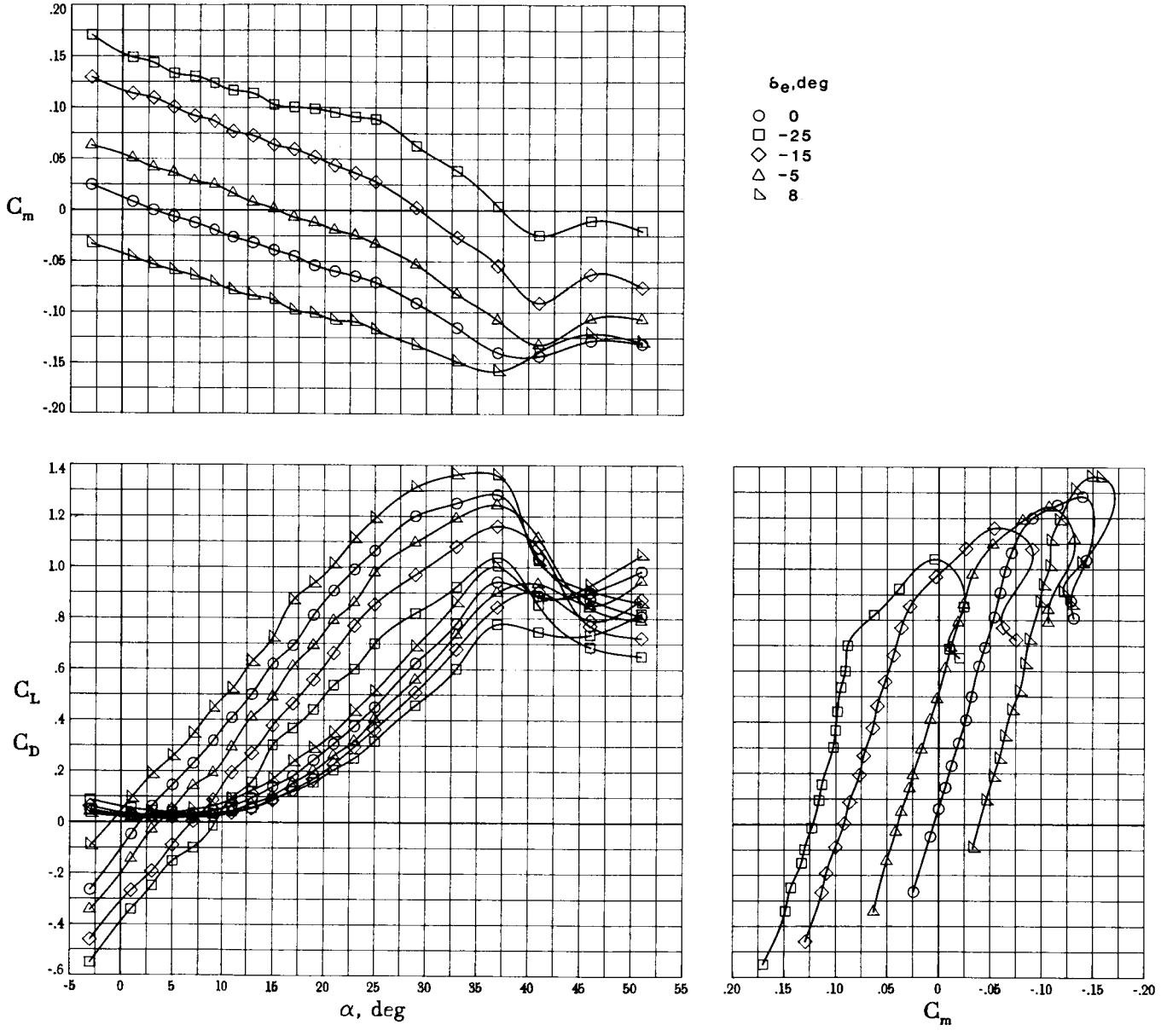

(a) Basic configuration.

Figure 12. Effect of elevator deflection on longitudinal aerodynamic characteristics of full-span constant-chord configuration with various leading-edge deflections. $\delta_a = 0°$; $\delta_r = 0°$.

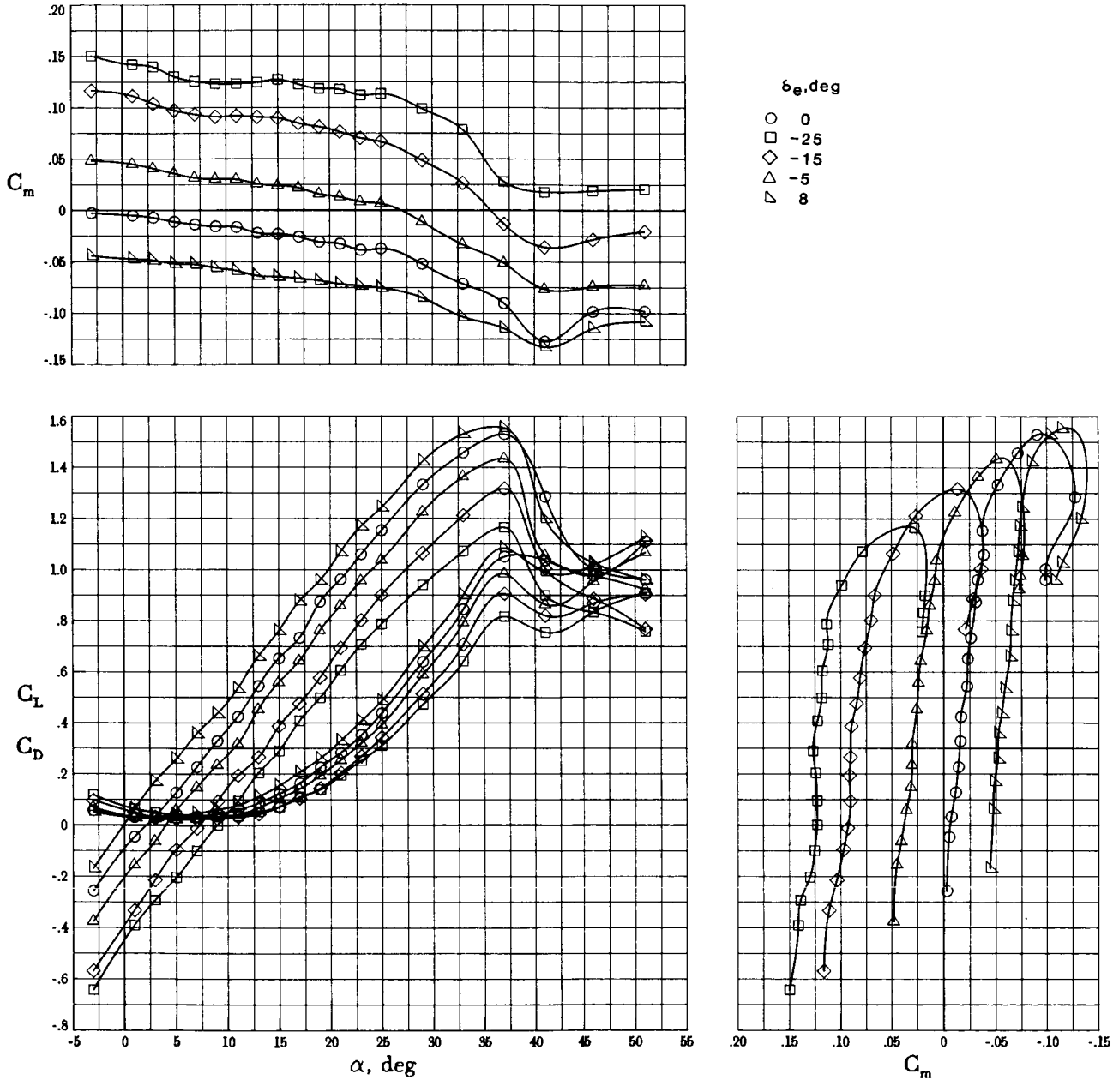

(b) $\delta_{f,le} = 30°$.

Figure 12. Continued.

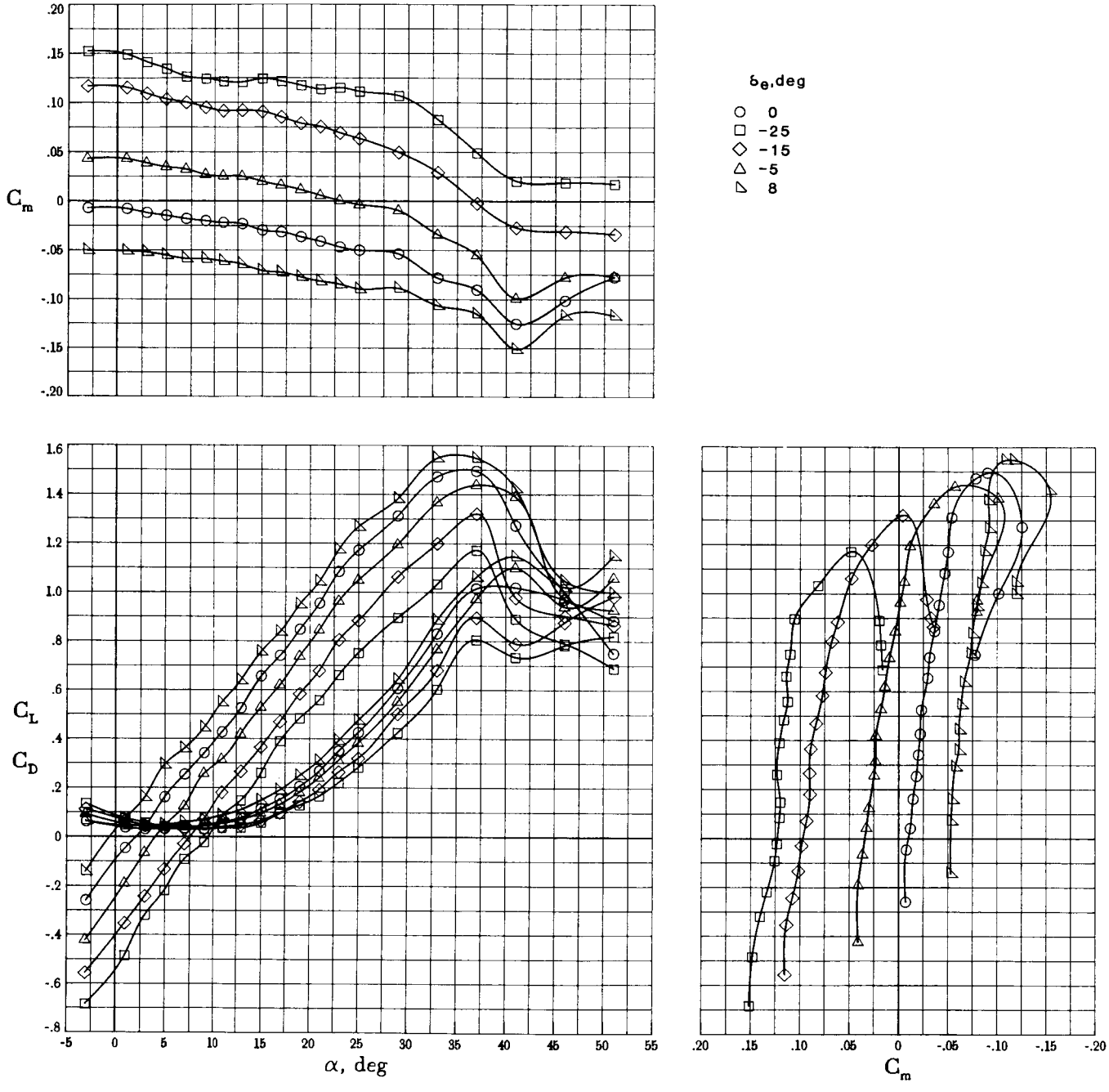

(c) $\delta_{f,le} = 40°$.

Figure 12. Continued.

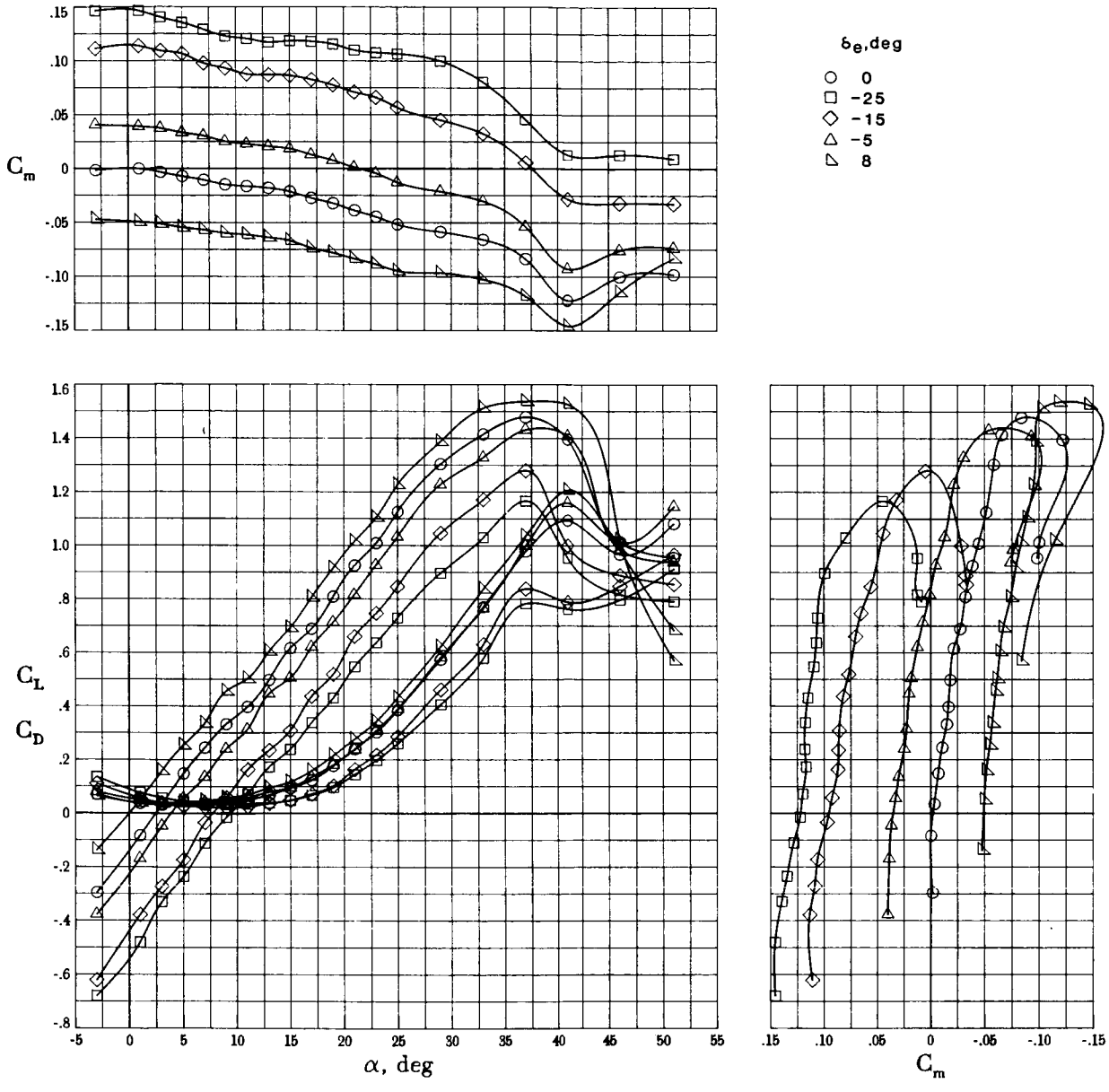

(d) $\delta_{f,le} = 50°$.

Figure 12. Concluded.

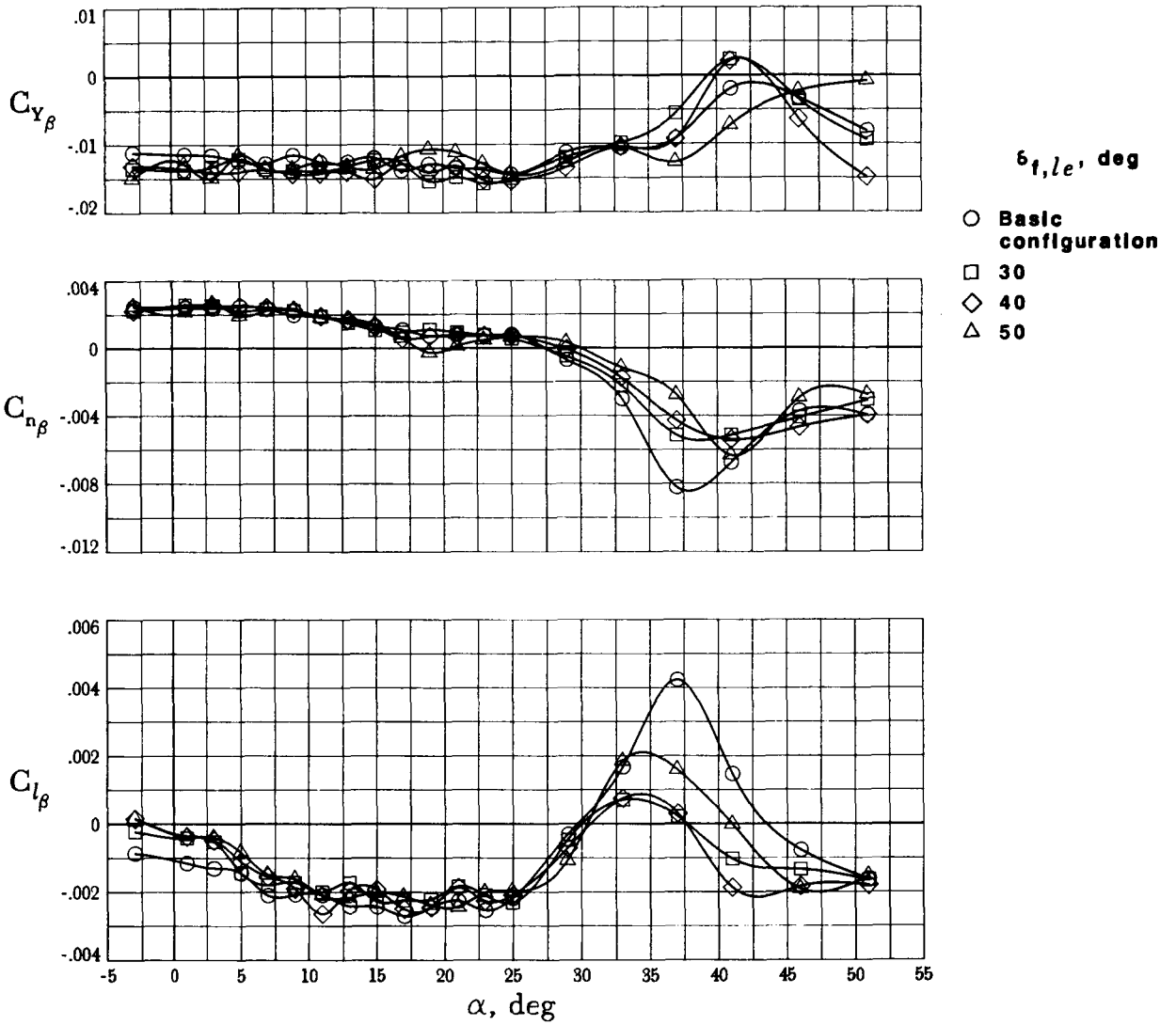

(a) Full-span gothic flap.

Figure 13. Effect of leading-edge flap deflection on lateral-directional stability of various vortex flap configurations.

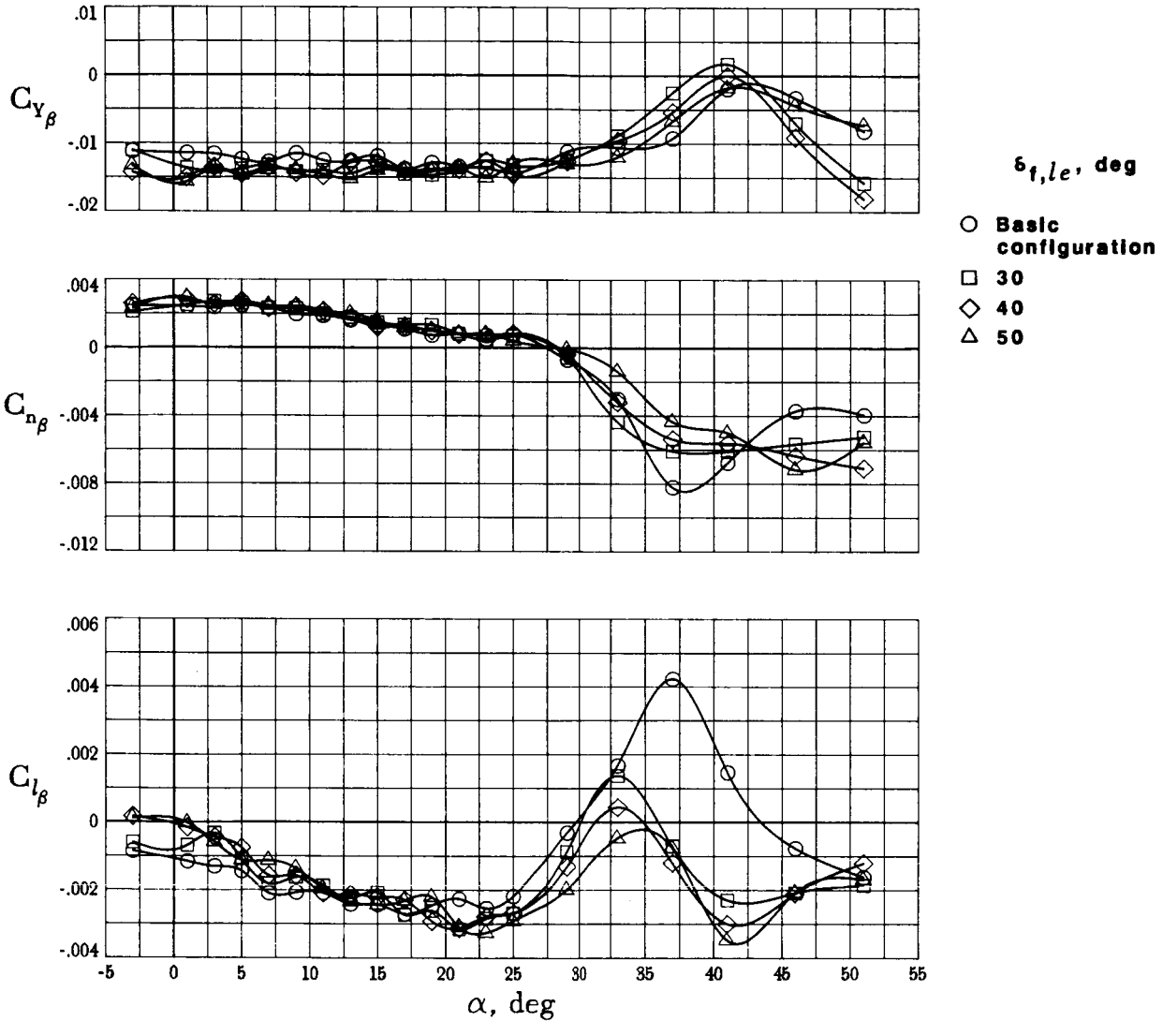

(b) Part-span flap.

Figure 13. Continued.

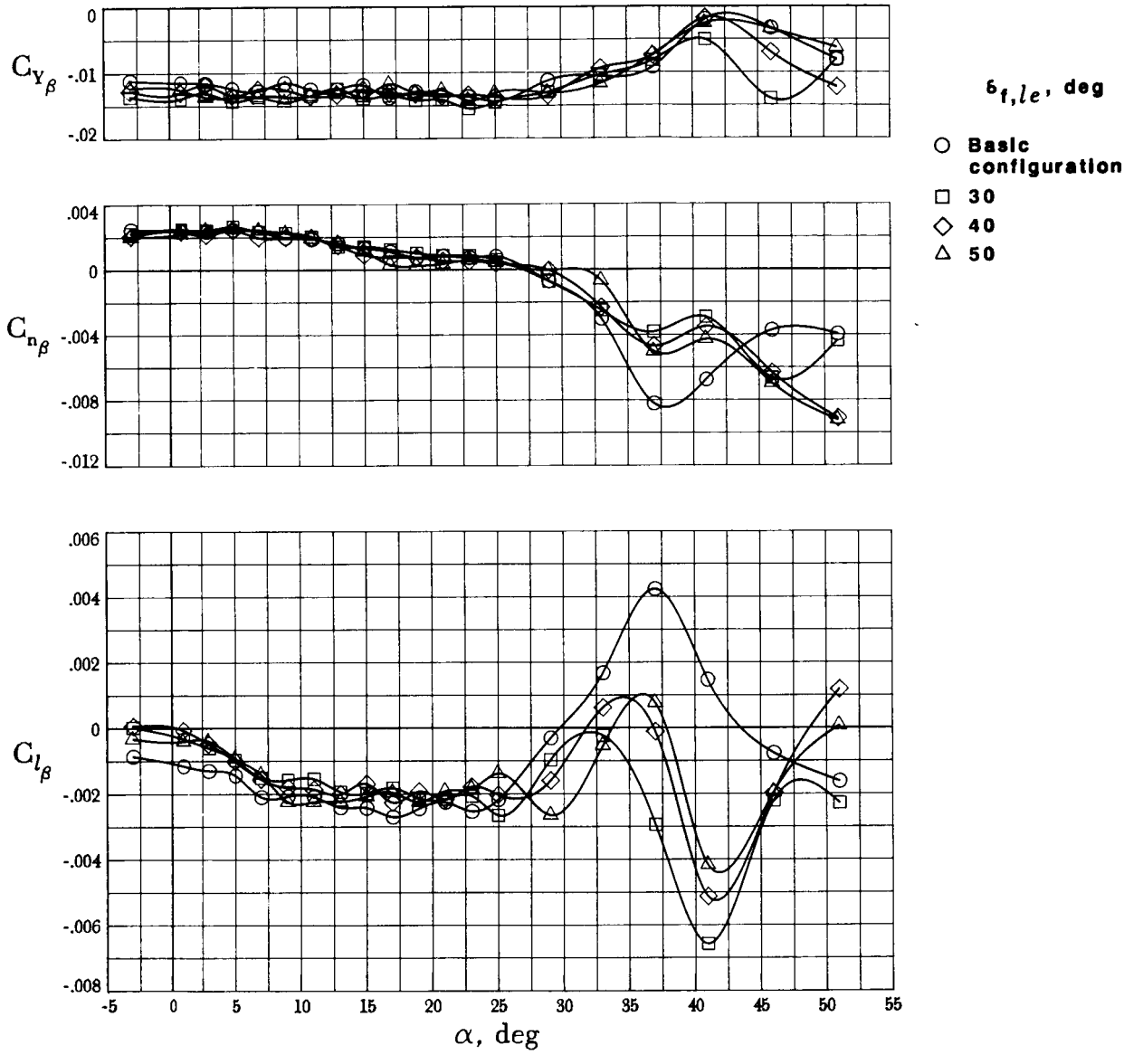

(c) Full-span constant-chord flap.

Figure 13. Concluded.

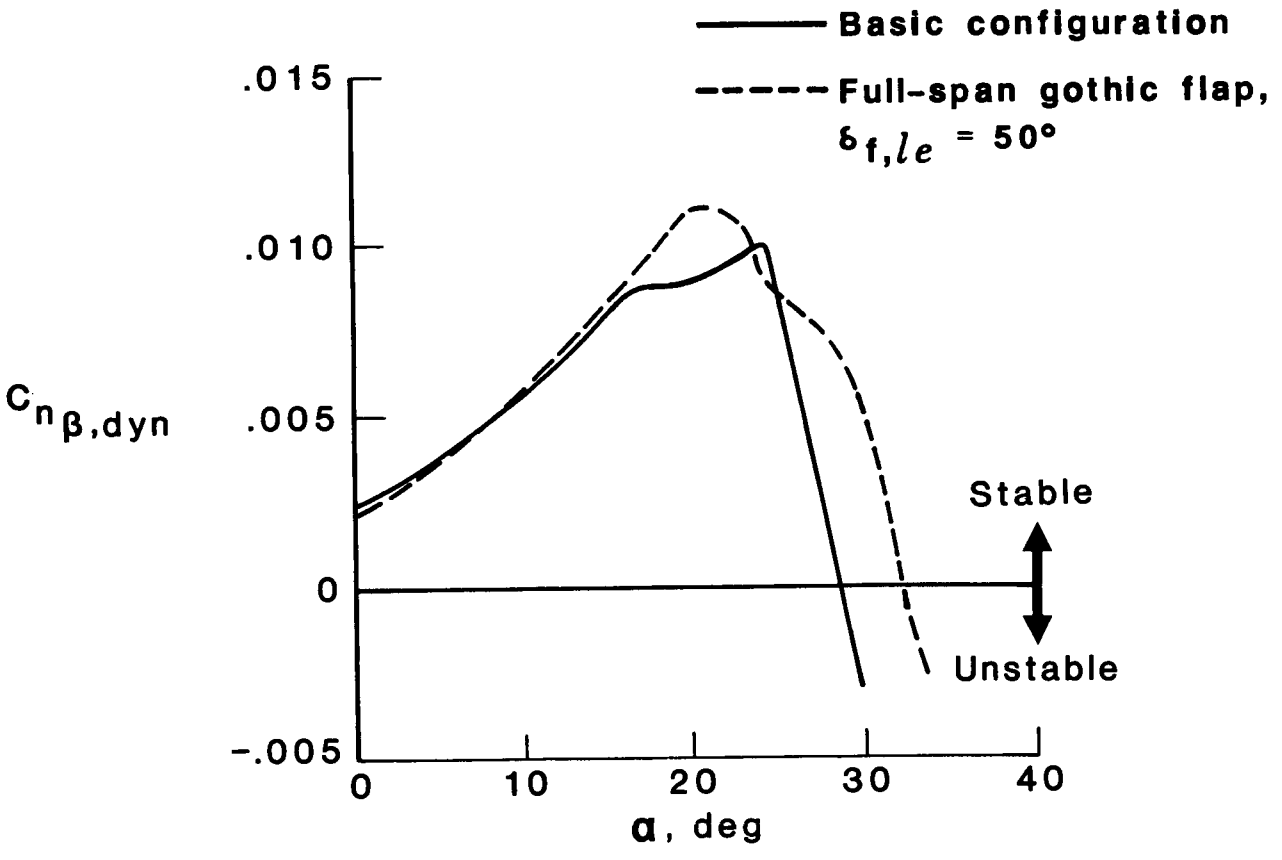

Figure 14. Effect of full-span gothic flap on the lateral-directional yaw divergence parameter $C_{n_{\beta,\mathrm{dyn}}}$.

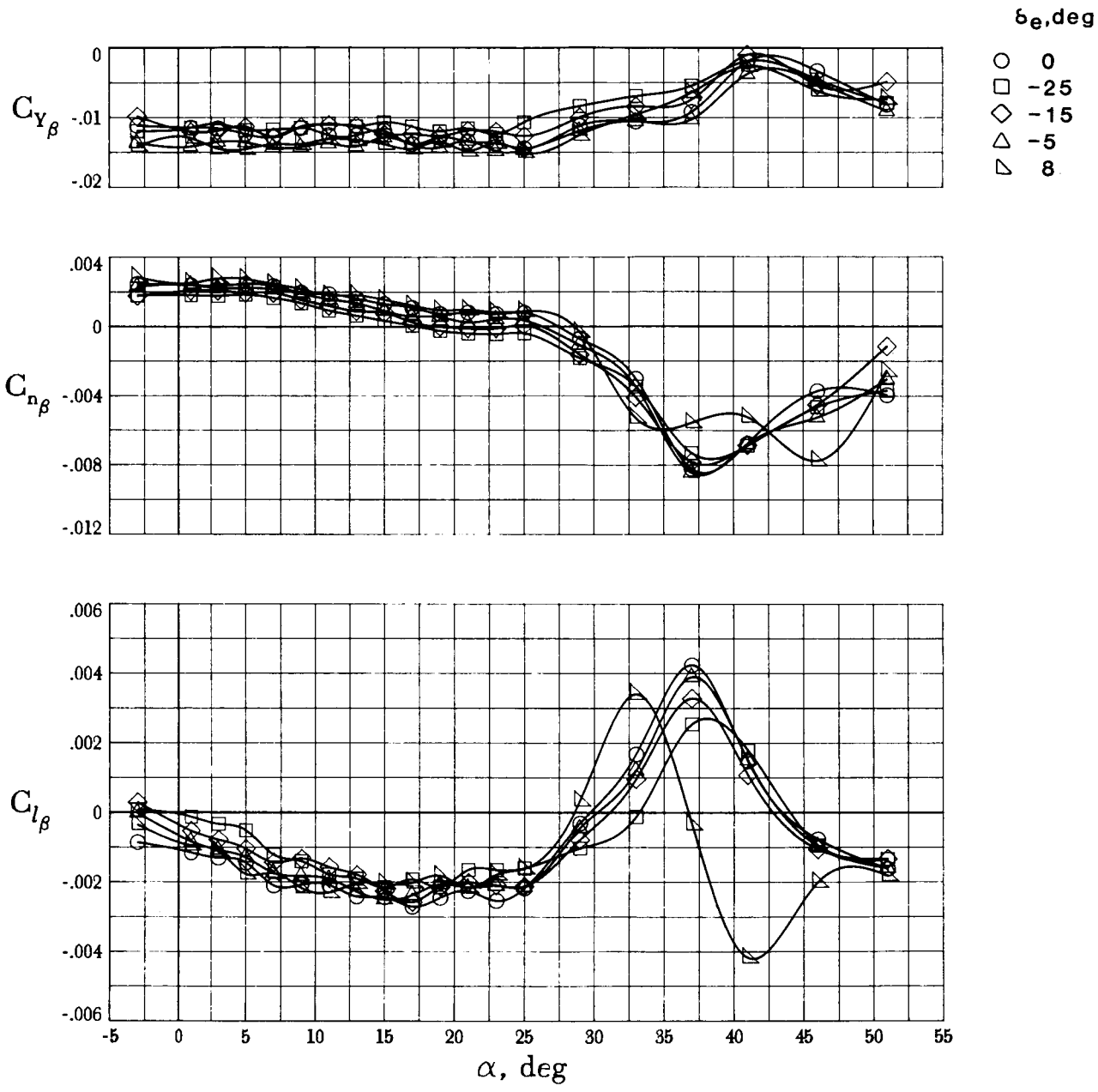

(a) Basic configuration.

Figure 15. Effect of elevator deflection on lateral-directional stability of full-span constant-chord flap configuration at various leading-edge flap deflections. $\delta_a = 0°$; $\delta_r = 0°$.

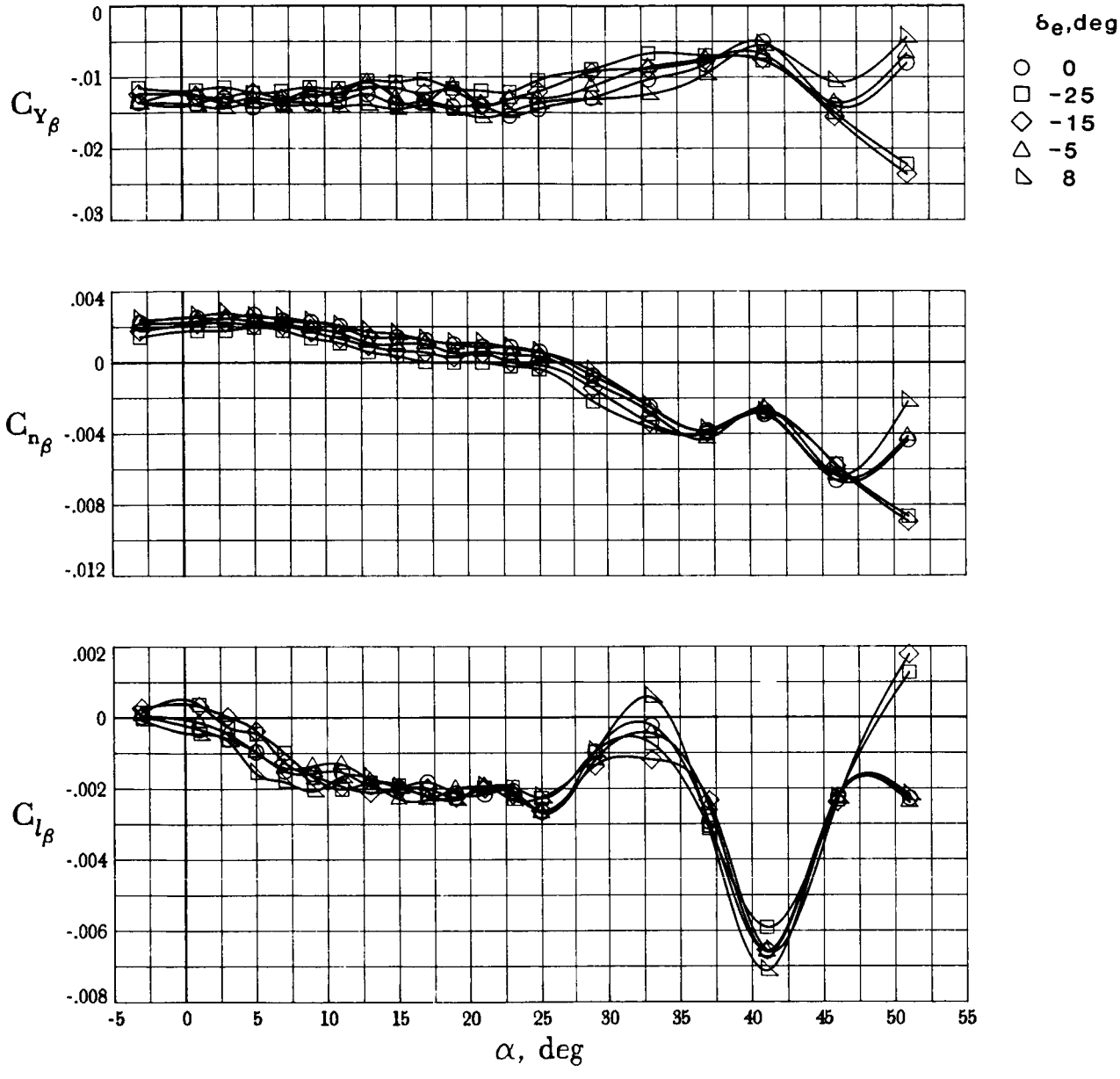

(b) $\delta_{f,le} = 30°$.

Figure 15. Continued.

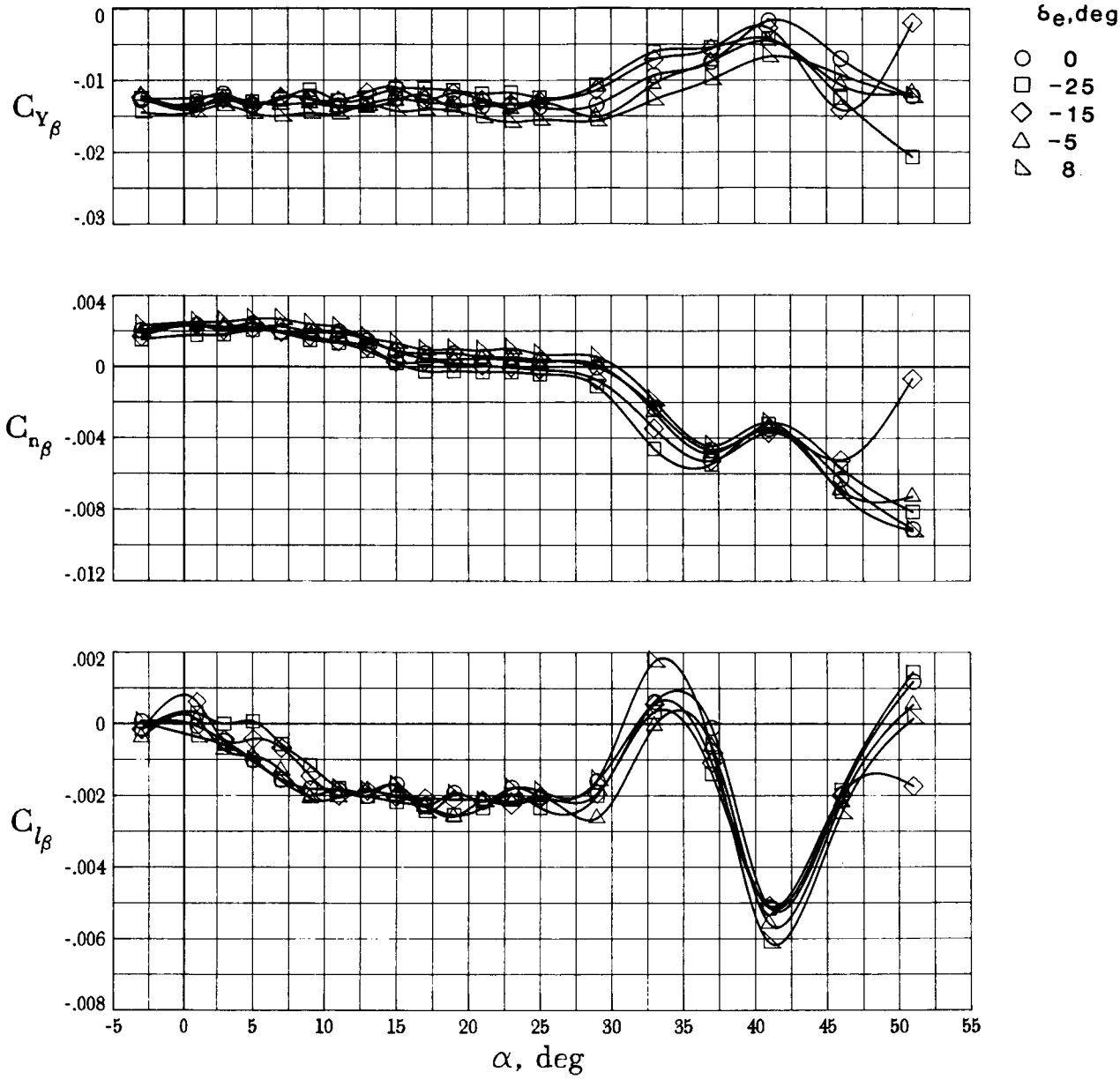

(c) $\delta_{f,le} = 40°$.

Figure 15. Continued.

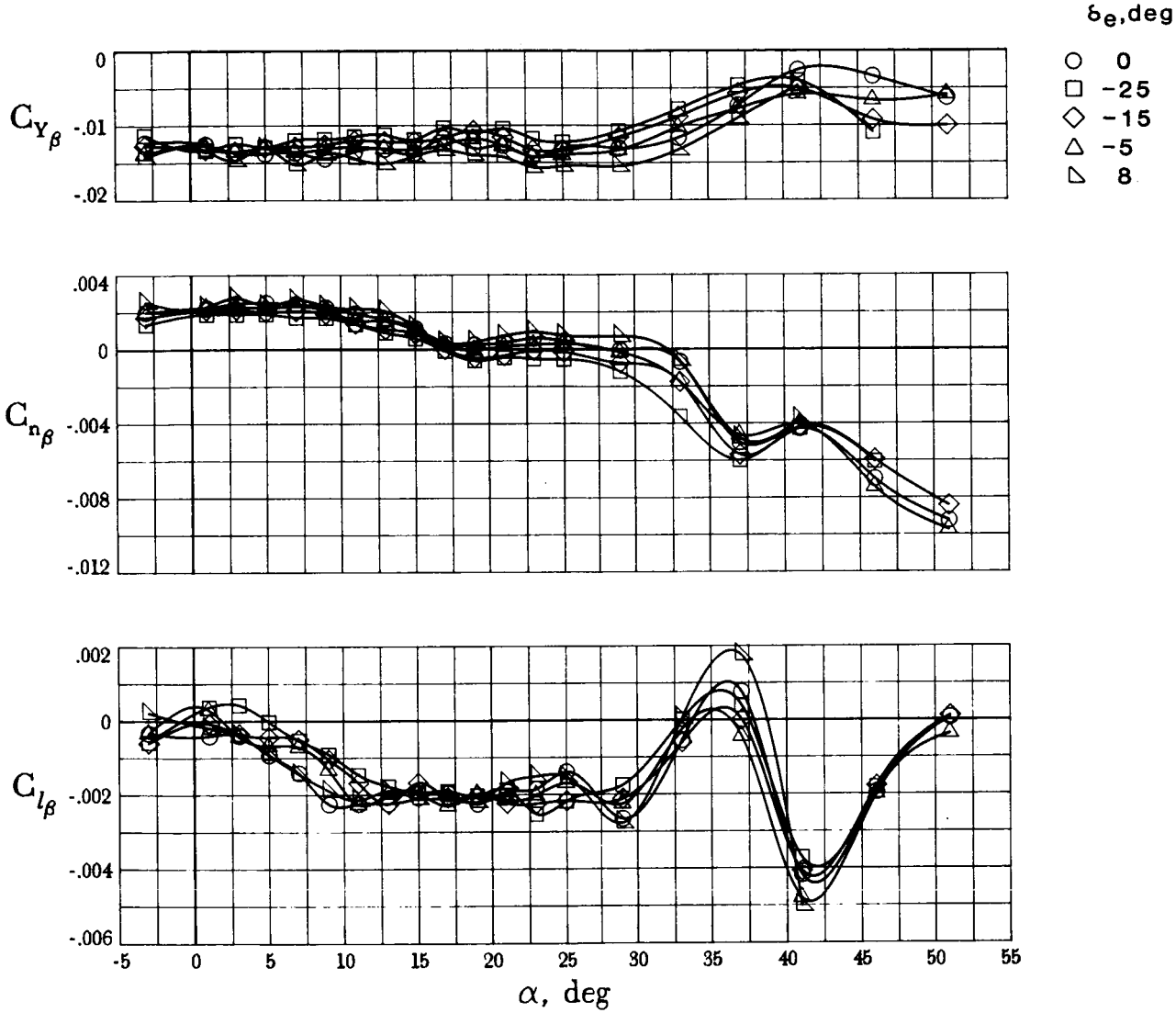

(d) $\delta_{f,le} = 50°$.

Figure 15. Concluded.

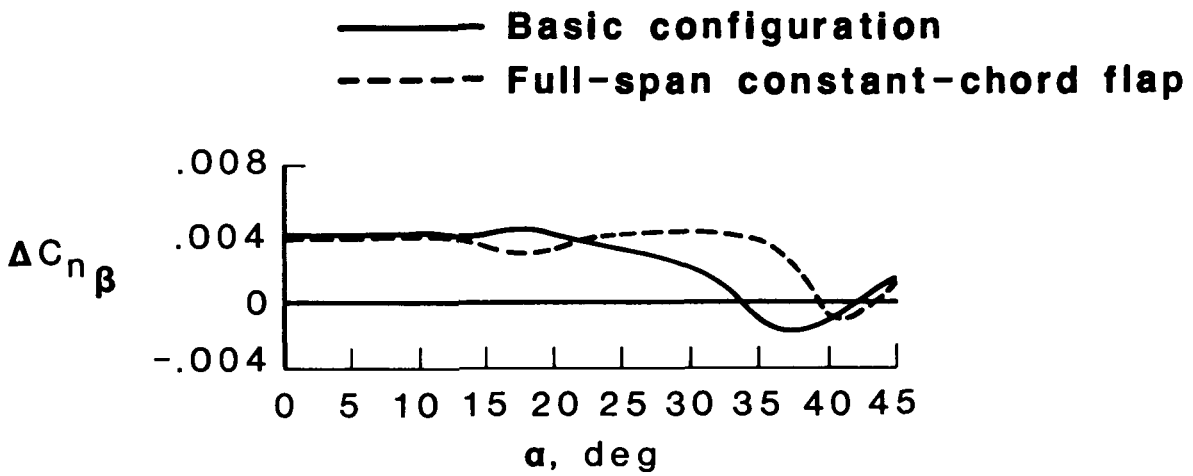

Figure 16. Effect of full-span constant-chord flap on directional stability provided by vertical tail. $\delta_{f,le} = 50°$.

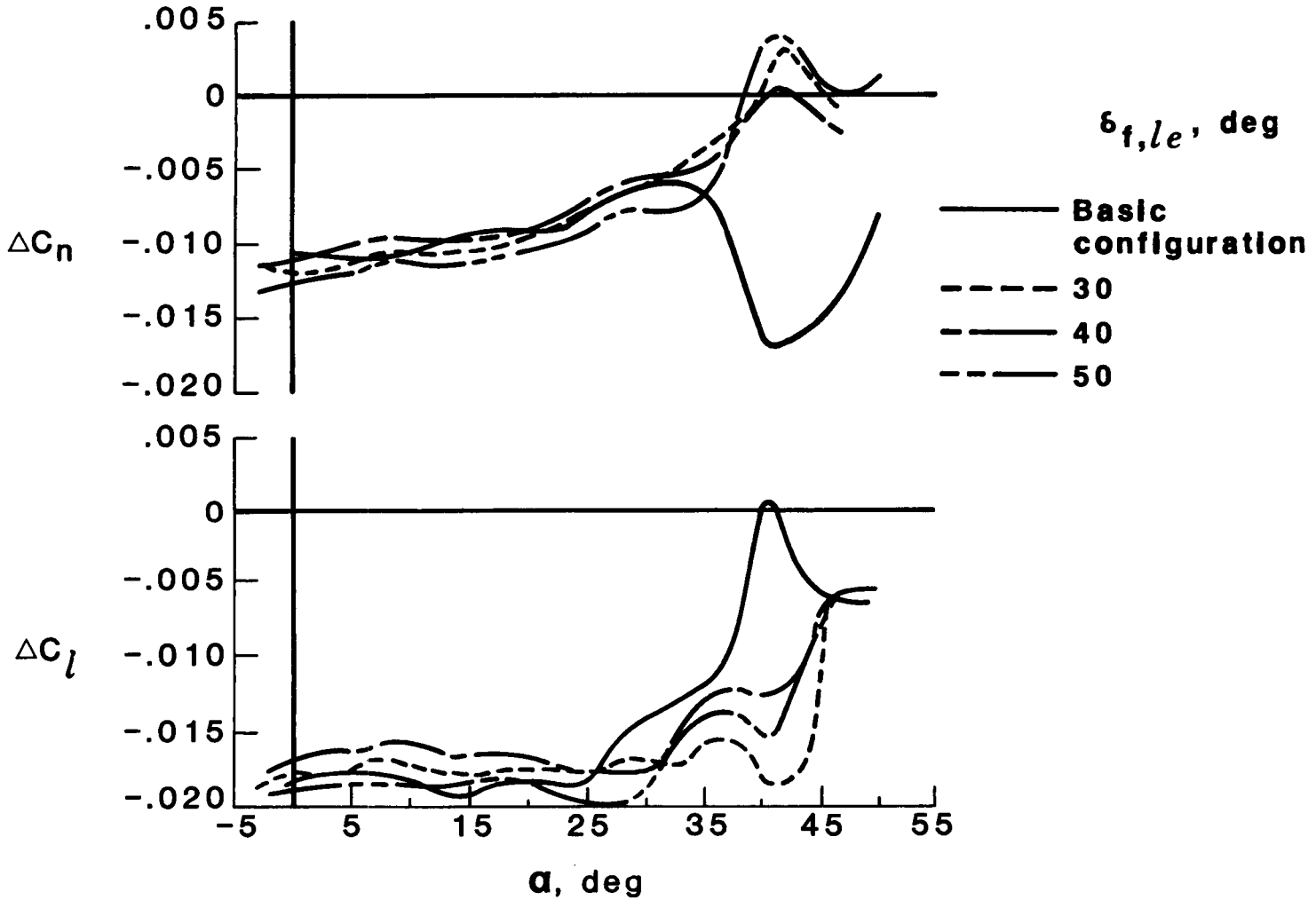

(a) $\delta_e = 0°$.

Figure 17. Effect of full-span constant-chord flap on aileron control power. $\delta_a = 7°$.

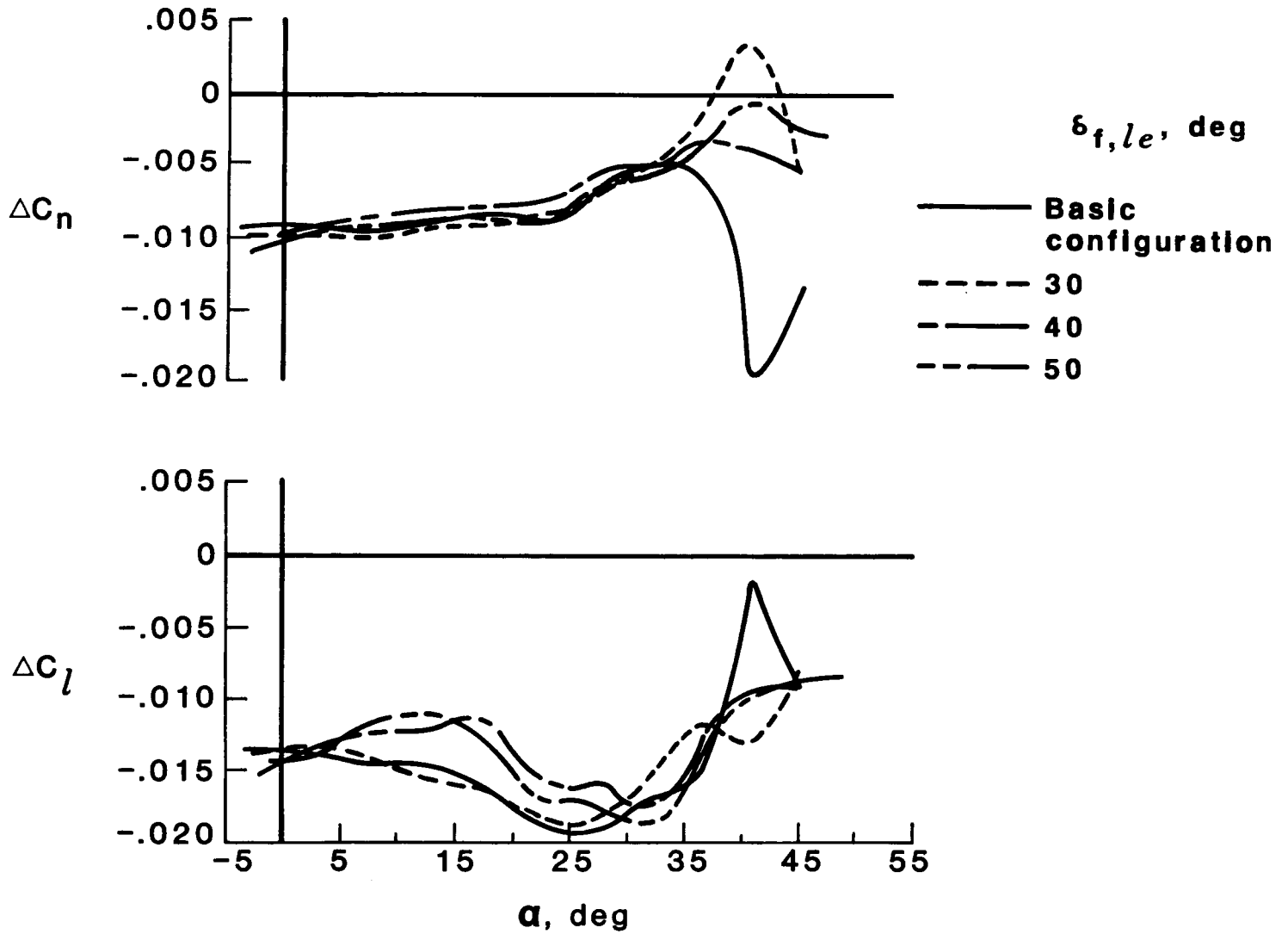

(b) $\delta_e = -15°$.

Figure 17. Concluded.

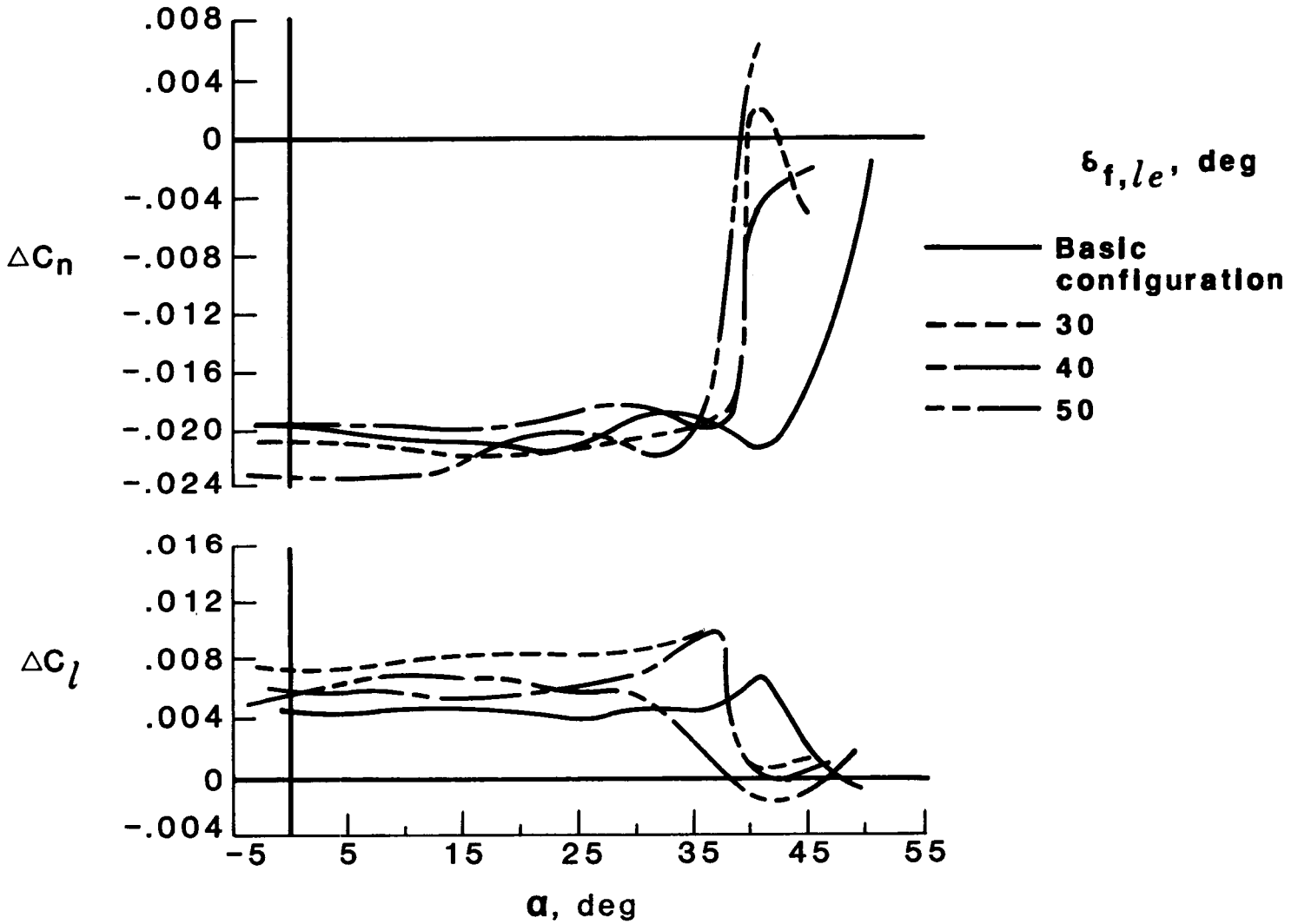

Figure 18. Effect of full-span constant-chord flap on rudder control power. $\delta_r = 25°$.

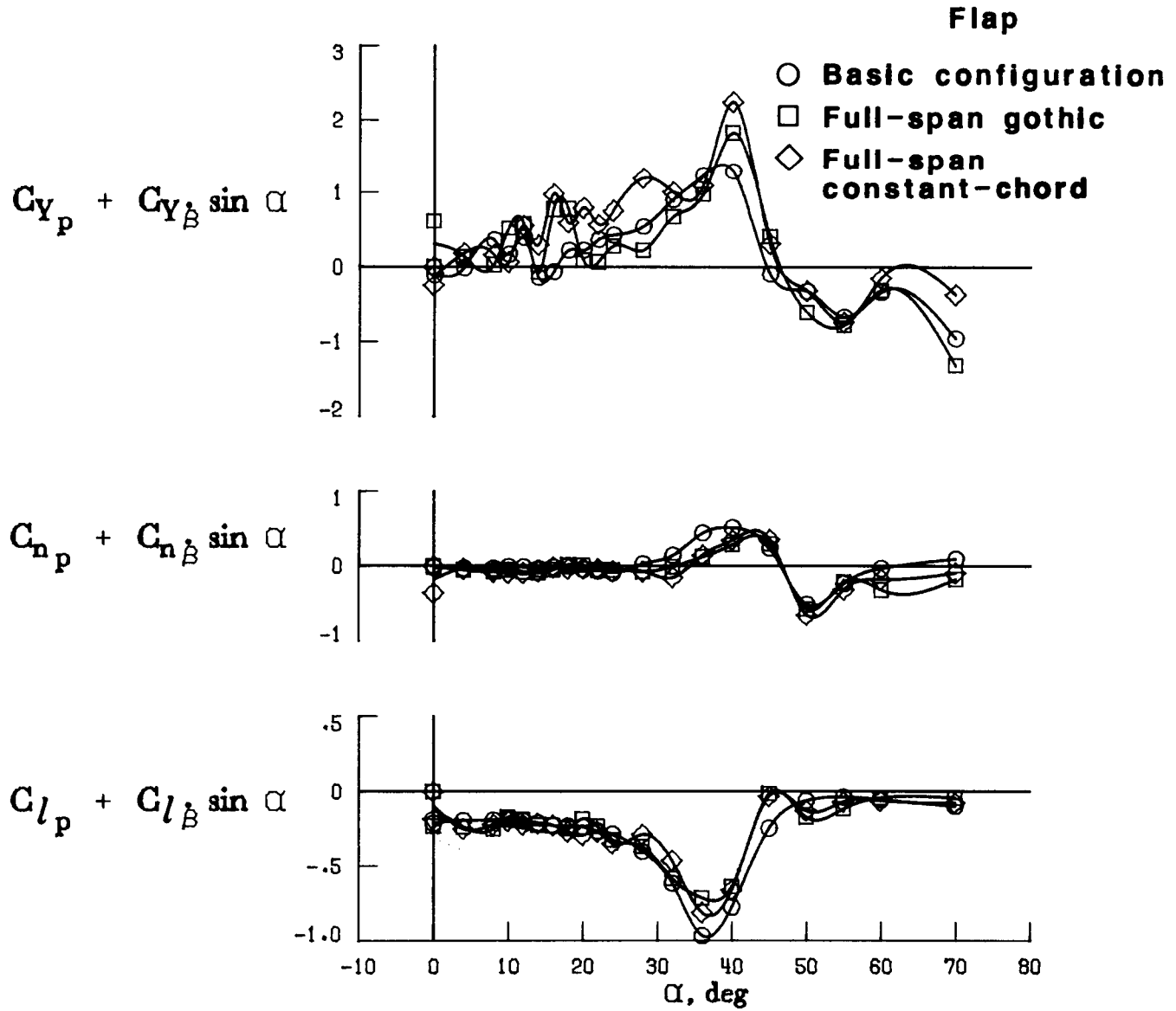

Figure 19. Effect of vortex flaps on dynamic roll stability derivatives. $\delta_{f,le} = 50°$.

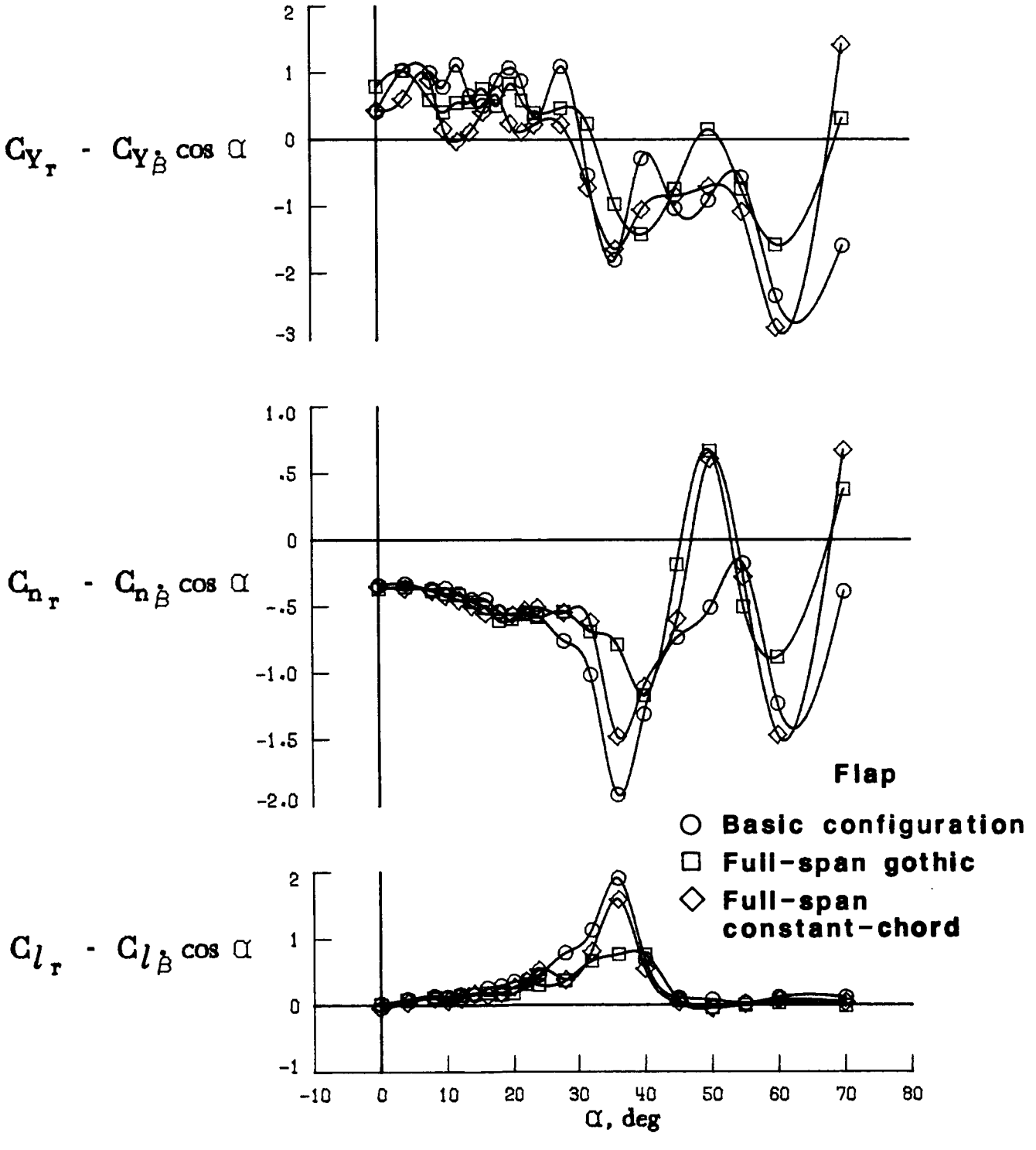

Figure 20. Effect of vortex flaps on dynamic yaw stability derivatives. $\delta_{f,le} = 50°$.

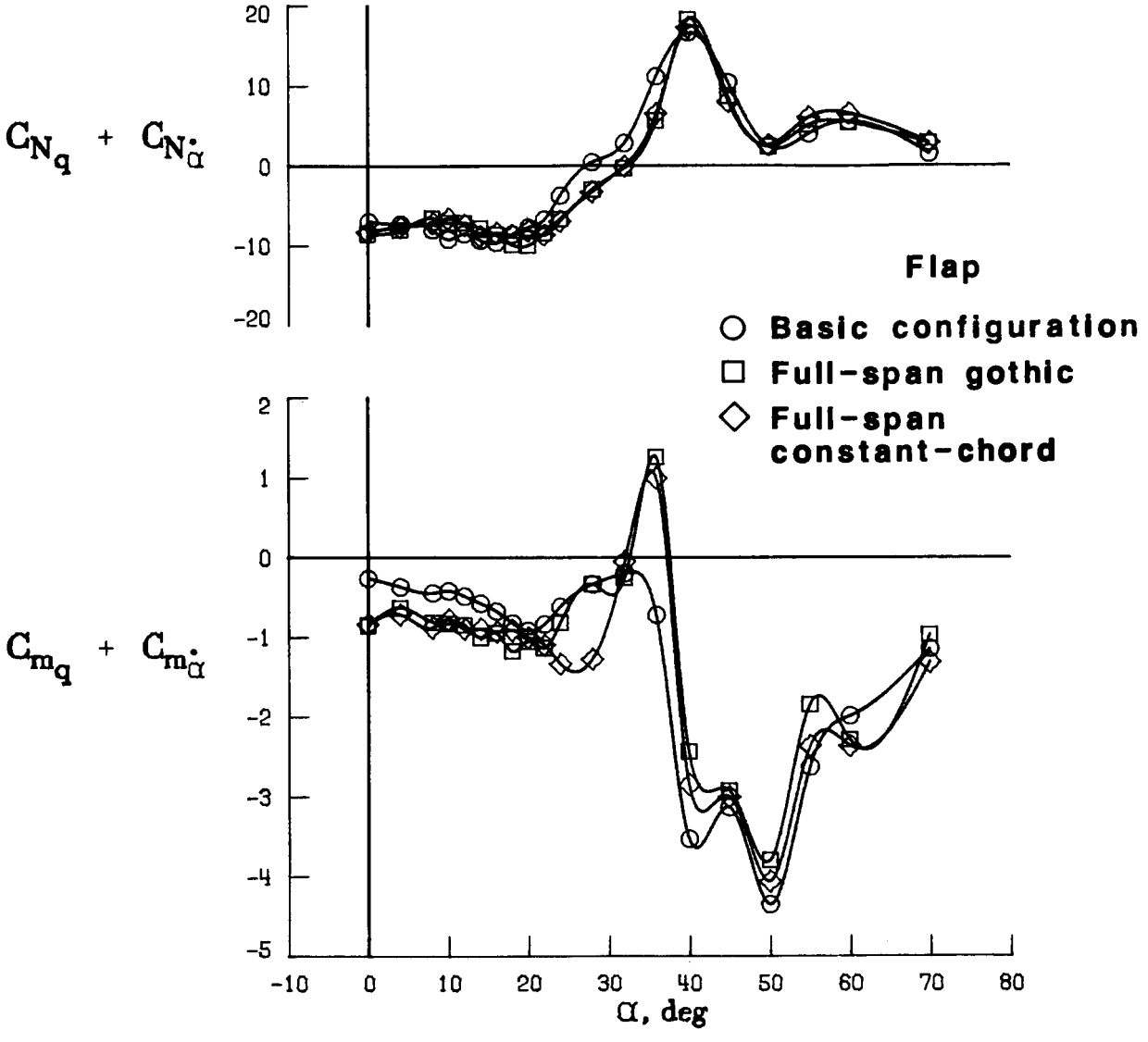

Figure 21. Effect of vortex flaps on dynamic pitch stability derivatives. $\delta_{f,le} = 50°$.

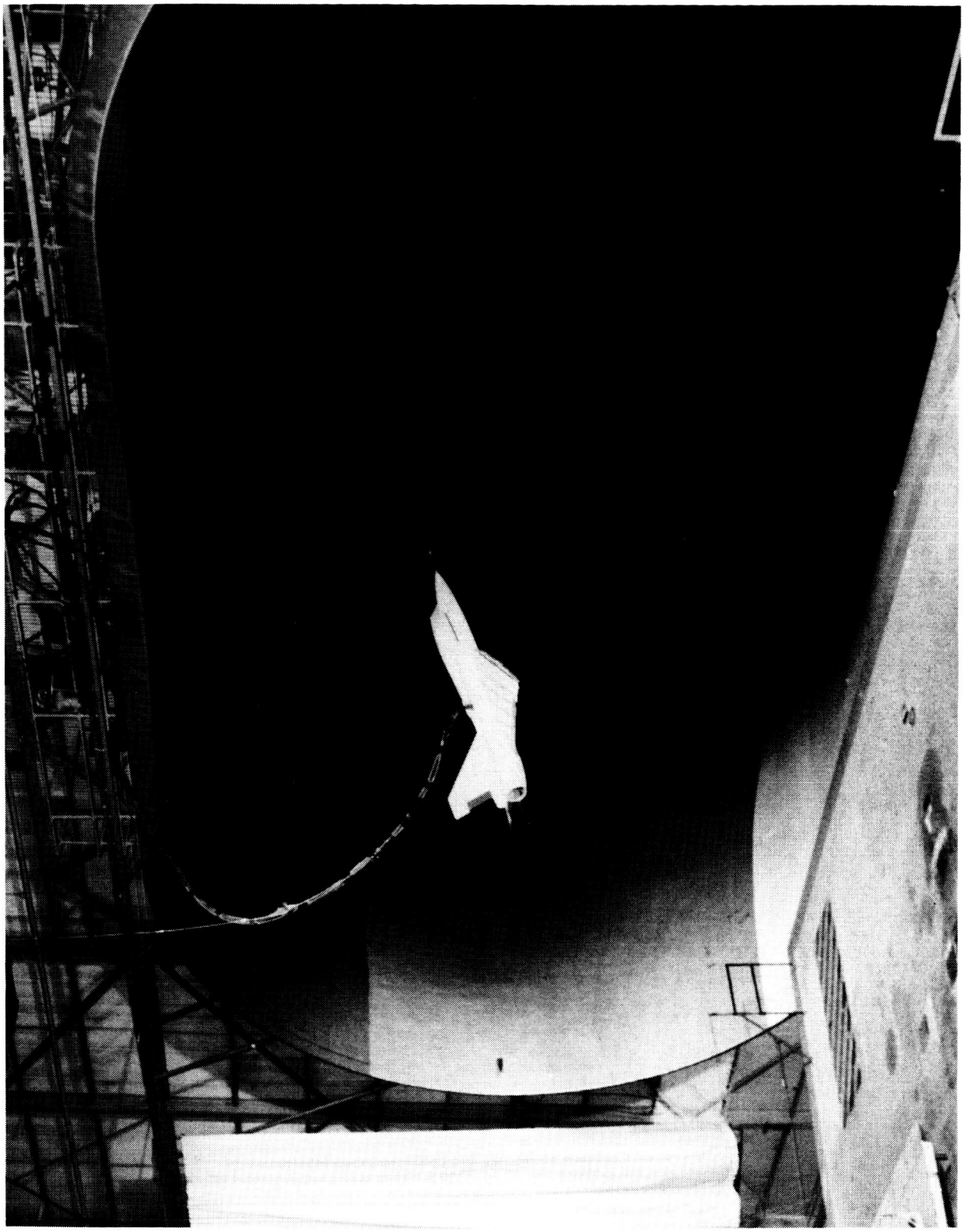

L-84-9804

Figure 22. Free-flight test of 0.15-scale model of F-106B airplane with full-span gothic flap. $\delta_{f,le} = 50°$.

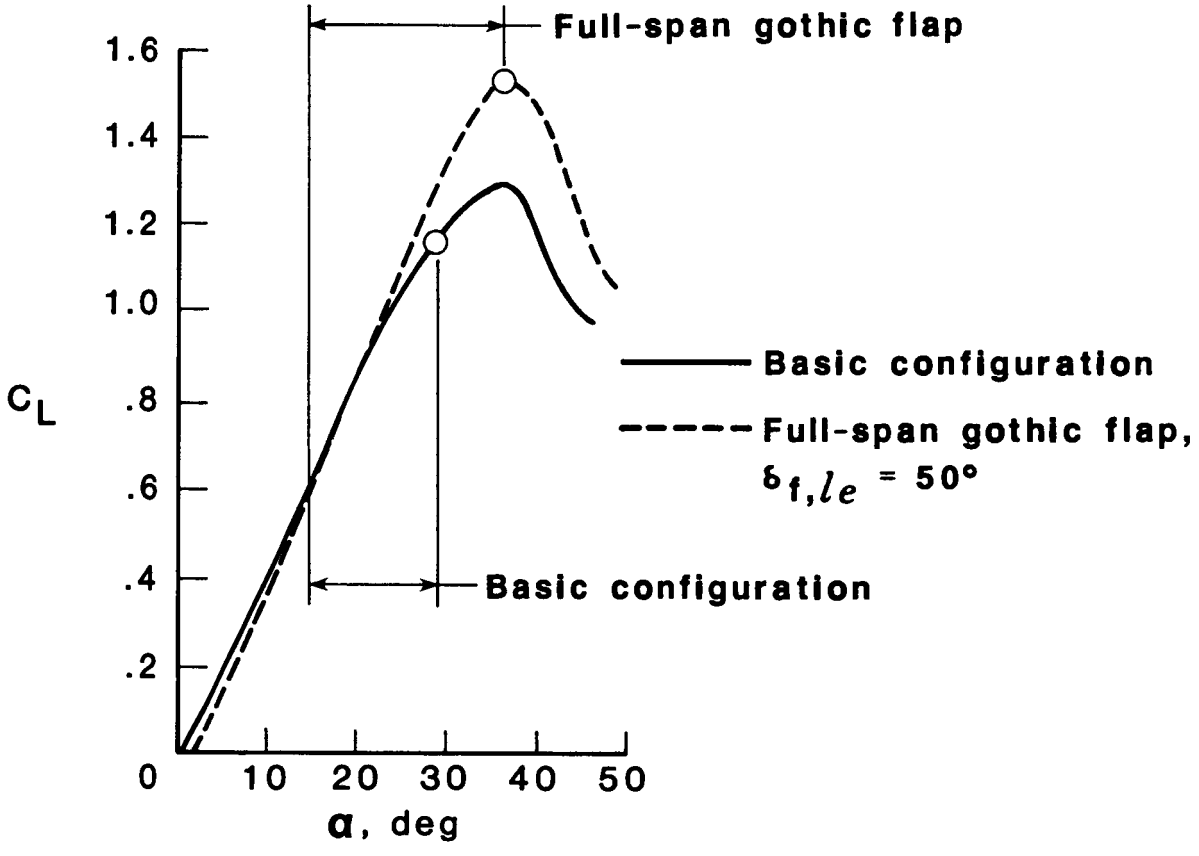

Figure 23. Angle-of-attack range of free-flight tests of 0.15-scale F-106B model.

NASA
National Aeronautics and Space Administration

Report Documentation Page

1. Report No.	2. Government Accession No.	3. Recipient's Catalog No.
NASA TP-2700		

4. Title and Subtitle	5. Report Date
Wind-Tunnel Free-Flight Investigation of a 0.15-Scale Model of the F-106B Airplane With Vortex Flaps	May 1987
	6. Performing Organization Code
7. Author(s)	8. Performing Organization Report No.
Long P. Yip	L-16202
9. Performing Organization Name and Address	10. Work Unit No.
NASA Langley Research Center Hampton, VA 23665-5225	505-61-41-01
	11. Contract or Grant No.
12. Sponsoring Agency Name and Address	13. Type of Report and Period Covered
National Aeronautics and Space Administration Washington, DC 20546-0001	Technical Paper
	14. Sponsoring Agency Code

15. Supplementary Notes

16. Abstract

An investigation to determine the effects of vortex flaps on the flight dynamic characteristics of the F-106B in the area of low-speed, high-angle-of-attack flight was undertaken on a 0.15-scale model of the airplane in the Langley 30- by 60-Foot Tunnel. Static force tests, dynamic forced-oscillation tests, as well as free-flight tests were conducted to obtain a data base on the flight characteristics of the F-106B airplane with vortex flaps. Vortex flap configurations tested included a full-span gothic flap, a full-span constant-chord flap, and a part-span gothic flap.

17. Key Words (Suggested by Authors(s))

Vortex flap
Free flight
High angle of attack
Dynamic stability
Stability and control

18. Distribution Statement

Unclassified—Unlimited

Subject Category 02

19. Security Classif.(of this report)	20. Security Classif.(of this page)	21. No. of Pages	22. Price
Unclassified	Unclassified	45	A03

For sale by the National Technical Information Service, Springfield, Virginia 22161-2171